Hindawi
Journal of Immunology Research
Volume 2022, Article ID 3393027, 32 pages
https://doi.org/10.1155/2022/3393027

Research Article

Cuproptosis-Related Signature Predicts the Prognosis, Tumor Microenvironment, and Drug Sensitivity of Hepatocellular Carcinoma

Xiangjun Qi,[1] **Jiayun Guo**,[1] **Guoming Chen**,[2] **Caishan Fang**,[1] **Leihao Hu**,[1] **Jing Li**,[3] **and Chi Zhang**[4]

[1]*The First Clinical School of Guangzhou University of Chinese Medicine, Guangzhou, China*
[2]*School of Chinese Medicine, Li Ka Shing Faculty of Medicine, The University of Hong Kong, Hong Kong S.A.R, China*
[3]*The First Hospital of Hunan University of Chinese Medicine, Changsha, China*
[4]*The Second Clinical School of Beijing University of Chinese Medicine, Beijing, China*

Correspondence should be addressed to Jing Li; lilee2711@sina.com

Received 13 June 2022; Revised 7 August 2022; Accepted 13 October 2022; Published 16 November 2022

Academic Editor: Anup Singh Pathania

Background. Copper (Cu) metabolism is strongly associated with liver disease. Cuproptosis is a novel format of cell death, and cuproptosis-related genes (CRGs) were identified. However, the role of CRGs in Hepatocellular Carcinoma (HCC) remains unknown. *Method*. The mRNA transcriptome profiling data, somatic mutation data, and copy number gene level data of The Cancer Genome Atlas-Liver Hepatocellular Carcinoma project (TCGA-LIHC) were downloaded for subsequent analysis. Molecular characterization analysis of CRGs, including differential gene expression analysis, mutation analysis, copy number variation (CNV) analysis, Kaplan-Meier analysis, and immune regulator prioritization analysis, was implemented. The nonnegative matrix factorization (NMF) approach was used to identify the CRG-related molecular subtypes. Principal component analysis was adopted to verify the robustness and reliability of the molecular subtype. The least absolute shrinkage and selection operator regression analysis was performed to construct the prognostic signature based on differentially expressed genes between molecular subtypes. The survival characteristics of the molecular subtype and the signature were analyzed. The Gene Set Variation Analysis was performed for functional annotation. The immune landscape analysis, including immune checkpoint gene analysis, single sample gene set enrichment analysis, tumor immune dysfunction and exclusion (TIDE) analysis, immune infiltration cell, and tumor mutation burden analysis (TMB), was conducted. The ability of the signature to predict conventional anti-HCC agent responses was evaluated. The signature was validated in the LIRI-JP cohort and the IMvigor210 cohort. *Result*. A total of 13 CRGs are differentially expressed between the tumor and normal samples, while the mutation of CRGs in HCC is infrequent. The expression of CRGs is associated with the CNV level. Fourteen CRGs are associated with the prognosis of HCC. Two clusters were identified and HCC patients were divided into 2 groups with a cutoff risk score value of 1.570. HCC patients in the C1 cluster and high-risk have a worse prognosis. The area under the receiver operating characteristic curve for predicting 1-, 2-, and 3-year overall survival is 0.775, 0.768, and 0.757 in the TCGA-LIHC cohort, and 0.811, 0.741, and 0.775 in the LIRI-JP cohort. Multivariate Cox regression analysis indicates that the signature is an independent prognostic factor. Pathways involved in metabolism and gene stability and immune infiltration cells are significantly enriched. Immune checkpoint genes are highly expressed in the C1 cluster. TMB is positively correlated with the risk score. HCC patients in the high-risk group are more likely to benefit from conventional anti-HCC agents and immune checkpoint inhibitor therapies. *Conclusion*. The molecular characterization of CRGs in HCC is presented in this study, and a successful prognostic signature for HCC based on the cuproptosis-related molecular subtype was constructed.

1. Introduction

Hepatocellular Carcinoma (HCC), which accounts for 75-85% of primary liver cancer cases, remains a major public health issue worldwide [1]. It is reported in the Global Cancer Statistics 2020 that the newly diagnosed cases and death cases of primary liver cancer are sorted by sixth and third, respectively. The 5-year survival rates in China and the United States are only 12.1% [2] and 18% [3]. HCC patients at an early stage can be cured by surgical interventions, whereas limited drugs are effective in advanced patients. Few molecular targeted drugs have been successfully applied to HCC except for several multikinase inhibitors and antiangiogenesis drugs, such as sorafenib and bevacizumab. What is more, sketchy molecular testing for directing HCC treatment has been conducted [4]. Immune checkpoint inhibitor (ICI) therapies have shown encouraging efficacy in advanced HCC patients. Atezolizumab combined with bevacizumab prolonged the median progression-free survival to 6.8 months [5]. Not only is ICI therapy facing resistant factors originating from the expression level of immune checkpoint point genes, tumor immune microenvironment, and tumor mutation burden (TMB) but also the specific molecular mechanisms remain unclear [6].

HCC is characterized by high heterogeneity, which influences tumor progression, aggression, and response to antitumor agents [7]. Gene changes such as somatic mutations, epigenetic variations, and large-scale genomic alterations contribute to the occurrence of heterogeneity and result in different molecular subtypes [8]. Differential expression of a heterogeneous genome brings out the discrepant biological behavior of tumor cells and their tumor microenvironment. Thus, RNA sequencing is a potent approach used to identify molecular subtypes. A number of studies have proved that gene expression profile-based signatures could predict the prognosis [9] and recurrence of HCC [10] as well as classify the tumor microenvironment [11].

Copper (Cu) metabolism, which has been identified to be associated with liver diseases, such as Wilson disease [12], liver cirrhosis [13], and HCC [14], is recently identified to be involved in cell death. Cuproptosis is a brand-new form of regulated cell death brought forward in 2022 [15]. It is distinct from all other known types of cell death, including apoptosis, ferroptosis, pyroptosis, and necroptosis. A series of cuproptosis-related genes (CRGs) were recognized through a genome-wide CRISPR/Cas9 screen by researcher [15]. Previous studies have demonstrated the prognostic value and molecular subtype of ferroptosis-related genes [16] and pyroptosis-related genes [17] in HCC. However, little is known about cuproptosis in this regard.

In this study, we recognized the cuproptosis-related molecular subtype of HCC and developed a cuproptosis-related prognostic signature.

2. Materials and Methods

2.1. Data Preparation. The mRNA transcriptome profiling of The Cancer Genome Atlas-Liver Hepatocellular Carcinoma (TCGA-LIHC) project with transcripts per million format was downloaded and further transformed by log2 $(x + 1)$. The mRNA transcriptome profiling of the LIRI-JP project with fragments per kilobase of exon per million fragments format was obtained from the International Cancer Genome Consortium website (ICGC, https://dcc.icgc.org/) [18], and subsequently transformed into transcripts per million format and normalized by log2 $(x + 1)$. Somatic mutation data with VarScan2 variant aggregation and masking format and copy number gene level data of the TCGA-LIHC project were obtained from the UCSC Xena website (https://xena.ucsc.edu/) [19]. The clinical data of the TCGA-LIHC project and the LIRI-JP project were downloaded from the TCGA website (https://portal.gdc.cancer.gov/) and the ICGC website, respectively. The mRNA transcriptome profiling and clinical data of the IMvigor210 study [20] were downloaded with the R IMvigor210CoreBiologies package. The clinical samples lacking survival state or overall survival (OS) were excluded. A gene list of CRGs was extracted from the research conducted by Tsvetkov et al., including 10 genes identified by whole genome CRISPR/Cas9 screen analysis, 3 Cu transporter-related genes, and 3 tricarboxylic acid cycle-related genes [15].

2.2. Molecular Characterization of CRGs in HCC

2.2.1. Differential Expression Analysis of CRGs. To identify the expression differences of CRGs between the normal and tumor samples, the R limma and ggpubr package were used to generate the boxplots for the comparison.

2.2.2. Mutation Analysis of CRGs. The mutation frequency and mutation type of CRGs were visualized by the R maftools package.

2.2.3. Copy Number Variation (CNV) Analysis of CRGs. The occurrence of CNV was presented in a barplot, and the distribution of CRGs in chromosomes was depicted by a circle plot with the R RCircos package. The CNV data was divided into three levels, including single deletion, normal, and single gain, and the correlations between these three categorical variables (CNV data and mRNA expression data) were tested.

2.2.4. Kaplan-Meier Analysis and Correlation Analysis of CRGs. To specify the prognostic value of single CRG in HCC, R limma, survival, and survminer packages were used for drawing the Kaplan-Meier (K-M) curve and statistical test. The correlations between expression levels of CRGs were calculated and visualized by the R igraph package.

2.3. Construction and Validation of Cuproptosis-Related Molecular Subgroup and Signature

2.3.1. Immune Regulator Prioritization Analysis of CRG Set. The CRG set prioritization module includes T cell dysfunction, T cell exclusion score, Cox proportional-hazards (Cox-PH) regression score in the immune checkpoint inhibitor (ICB) cohort, and log-fold change (logFC) in CRISPR screens was established with the usage of the Tumor Immune Dysfunction and Exclusion (TIDE) website (http://tide.dfci.harvard.edu/). The T dysfunction score and

T cell exclusion score indicate the interactions between gene expression level and cytotoxic T cells as well as gene expression level and immunosuppressive cells [21]. The Cox-PH score was associated with ICB therapy response, and the logFC score was employed to sift genes that can interact with lymphocyte-mediated tumor killing [21].

2.3.2. Construction of Cuproptosis-Related Molecular Subtype. The nonnegative matrix factorization (NMF) approach, an unsupervised clustering analysis method, was performed to identify the presence of underlying molecular subgroups associated with cuproptosis. The R NMF package was employed in this process, and the detailed method used in NMF-clustering analysis was "brunet." The consensus matrix heat map and cophenetic correlation coefficient were used to determine the cluster number. Principal component analysis (PCA) was adopted to verify the robustness and reliability of the molecular subtypes.

2.3.3. Construction of Cuproptosis-Related Signature. Differential gene expression analysis was initially conducted for the molecular subgroups obtained from the NMF-clustering analysis. Differentially expressed genes (DEGs) among subtypes were screened with a threshold value $|\log FC| = 0.585$ and adjusted p value =0.05. Univariate Cox analysis was performed on DEGs and DEGs with a p value <0.05 were retained for subsequent analysis. The least absolute shrinkage and selection operator (LASSO) regression analysis with a repeated time of 1000 was used to improve the model stability. Multivariate Cox analysis was performed based on DEGs after LASSO regression analysis. Finally, a risk score for each patient was calculated using the following formula:

$$\text{RiskScore} = \sum_{i=1}^{n} \beta i Si. \quad (1)$$

The "βi" and the "Si" in the formula represent the coefficient and expression level of genes, respectively. Patients were divided into high- and low-risk groups according to a cutoff point generated by the Akaike information criterion (AIC). R survival, survminer, and glmnet packages were used in this section.

2.3.4. Correlations between Molecular Subtype and Signature. The differences in risk scores between the molecular subtypes were analyzed with a statistical test using the R ggpubr package. A Sankey diagram was plotted to show the distribution of patients by molecular subtype, risk score, and survival status.

2.3.5. Survival and Clinical Characteristics of Molecular Subtype and Signature. A K-M analysis was conducted to compare the survival curve between the molecular subtype and the risk score group. The differences in the clinical phenotype, including age, gender, histologic grade, and TNM stage, were measured as well. Receiver Operating Characteristic (ROC) curves were used to test the diagnostic performance of the signature. The ROC curves for 1-, 2-, and 3-year were plotted and further compared with the clinical ROC curve. Univariate and multivariate Cox regression analyses were adopted to determine whether the signature could be regarded as an independent prognostic factor. R packages including survival, pheatmap, pbapply, survivalROC, survminer, glmnet, and ggupbr were used for these operations.

2.3.6. Differential Gene Expression Analysis of CRGs. In order to recognize the different expression of CRGs between the molecular subtypes and the risk groups, we used the R limma and the ggpubr package to generate the boxplots for the comparison.

2.3.7. Gene Set Variation Analysis (GSVA) and Functional Enrichment. GSVA analysis was conducted to identify the biological pathway differences between the molecular subtypes and the risk groups. The KEGG subset file with gene symbol format was downloaded from the MSigDB database (https://www.gsea-msigdb.org/gsea/msigdb/). The threshold values used to screen significantly differentially enriched pathways were set as follows: adjusted p value =0.05. R limma, GSEABase, GSVA, and pheatmap package were utilized.

2.3.8. Immune Landscape of Molecular Subtype and Signature. The HCC-related immune checkpoint genes were extracted from Harkus et al.'s study, [6] and the expression levels of them were compared in accordance with diverse molecular subtypes and risk groups. The single sample gene set enrichment analysis (ssGSEA) algorithm was used to evaluate the immune cells and immune functions in tumor immune microenvironment. The infiltration abundance level of 23 types of immune cells and enrichment level of 13 types of immune functions was calculated and compared between the groups. The TIDE score, including dysfunction, exclusion, integrated TIDE score, and microsatellite instability (MSI) score of each HCC sample, were computed on the TIDE website. To evaluate the ratio of immune-stromal components in the tumor microenvironment, the R estimate package was utilized to calculate the StromalScore, ImmuneScore, and ESTIMATEScore. The immune scores were further compared between the groups. Moreover, the correlation between risk score and tumor-infiltrating immune cells, whose infiltration level was estimated by 7 algorithms including TIMER [22], quanTIseq [23], EPiC [24], CIBERSORT [25], xCell [26], MCP-counter [27], and CIBERSORT-ABS [28], was tested. The correlation between risk score and tumor mutation burden (TMB) was also tested.

2.3.9. Anti-HCC Agent Response Prediction. Gene expression and drug sensitivity data used for drug response prediction were downloaded from the Genomics of Drug Sensitivity in Cancer website (GDSC, https://www.cancerrxgene.org). The R package pRRophetic was utilized to calculate the half-maximal inhibitory concentration (IC_{50}) of 4 conventional anti-HCC agents, including sorafenib, cisplatin, paclitaxel, and gemcitabine, for each TCGA-LIHC project sample. The difference in IC_{50} between high- and low-risk groups was compared.

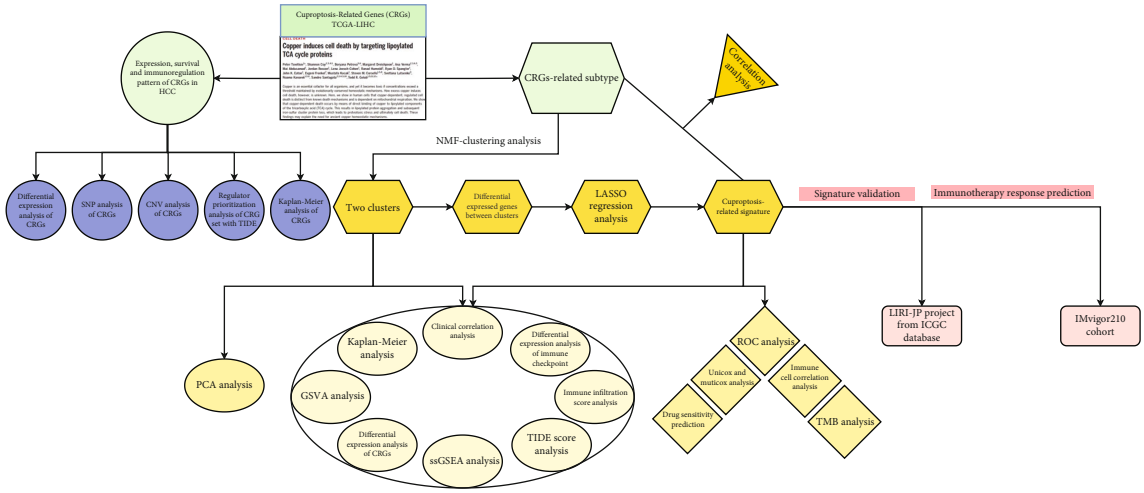

Figure 1: Overall design of the study.

2.3.10. Validation of the Constructed Signature. The LIRI-JP cohort was used to validate the constructed signature. A K-M analysis was conducted to compare the survival between the low-risk and the high-risk patients in the LIRI-JP cohort. A ROC diagram was plotted, and a corresponding area under curve (AUC) value was calculated to evaluate the accuracy of the signature. Univariate and multivariate Cox regression analyses were adopted to determine whether the signature could be regarded as an independent prognostic factor in the LIRI-JP cohort. The ability of the signature to predict ICIs' response was evaluated in the IMvigor210 cohort. The distribution of risk scores and risk status between complete response (CR)/partial response (PR) and stable disease (SD)/progressive disease (PD) was compared.

2.3.11. Statistical Analysis. All statistical operators were conducted with R 4.0.3 software. A log-rank test was used to compare the differences between the survival curves generated by K-M analysis. The comparison and correlation analysis in continuous data were the Wilcox test and the Spearman test. Differences in categorical data were compared using χ^2 or the Kruskal test. A p value below 0.05 was considered a statistically significant difference.

3. Results

A total of 424 mRNA transcriptome samples, which consist of 374 cancer and 50 normal samples, were obtained from the TCGA-LIHC project, as well as 371 clinical samples were retained after filtration. There were 231 HCC samples enrolled from the ICGC database and 381 ICI-treated tumor samples enrolled from the IMvigor210 cohort for validation. Figure 1 presents the overall design of the study.

3.1. Identification of Differentially Expressed, Prognosis-Related, and Immune-Related CRGs in HCC. A total of 16 CRGs were obtained from Tsvetkov et al.'s study, and their molecular characteristics are presented in Figure 2. The expression level of DBT and SLC31A1 in normal samples is significantly higher than in tumor samples, while LIPT1, LIAS, DLD, DLST, DLAT, PDHA1, PDHB, ATP7A, MTF1, GLS, and CDKN2A are the opposite (Figure 2(a)). The incidence of mutation in CRGs in HCC is 6.04% and is dominated by missense mutations (Figure 2(b)). CDKN2A is the most mutated gene among CGRs. ATP7A and CDKN2A, which are located on chromosomes X and 6, respectively, harbor a high frequency of CNV-deletion (Figures 2(c) and 2(d)). Supplementary Figure 1 indicates that the occurrence of CNV in DLAT, CDKN2A, PDHB, DLST, ATP7B, GCSH, MTF1, LIAS, FDX1, DBT, DLD, and GLS is significantly associated with gene expression levels. The K-M analysis of single CRG demonstrates that the overall survival of HCC patients in high expression level of ATP7B, FDX1, and SLC31A1 are superior to those in the low expression group (Figure 3(a)). High expression levels of ATP7A, CDKN2A, DLAT, DLD, DLST, GCSH, GLS, LIPT1, MTF1, PDHA1, and PDHB are the risk factors for HCC patients (Figures 3(a) and 3(b)). TIDE analysis of CRG set indicates that the low expression levels of GCSH and PDHA1 is associated with the T cell dysfunction in all datasets catalogued (Figure 3(c)), while the high expression levels of GCSH and PDHA1 are associated with the response of immune checkpoint inhibitors in Miao et al. [29] and Rizvi et al. [30]. The majority of CRGs are differentially expressed between normal and tumor samples and are associated with the prognosis of HCC, which suggests that CRGs are of importance in the development and progression of HCC.

3.2. Construction and Validation of CRG-Related Molecular Subtype

3.2.1. Differentially Expressed CRGs and Survival Differences between the Molecular Subtypes. Two clusters were identified after NMF-clustering analysis (Figure 4(a) and Supplementary Figure 2). The PCA analysis shows that HCC samples are distinctly separated into two clusters (Figure 4(b)). The K-M analysis between the C1 and the C2 suggests that the overall survival of patients in C2 is better than in C1 (Figure 4(c)). CRGs including FDX1, LIAS, DBT, DLST,

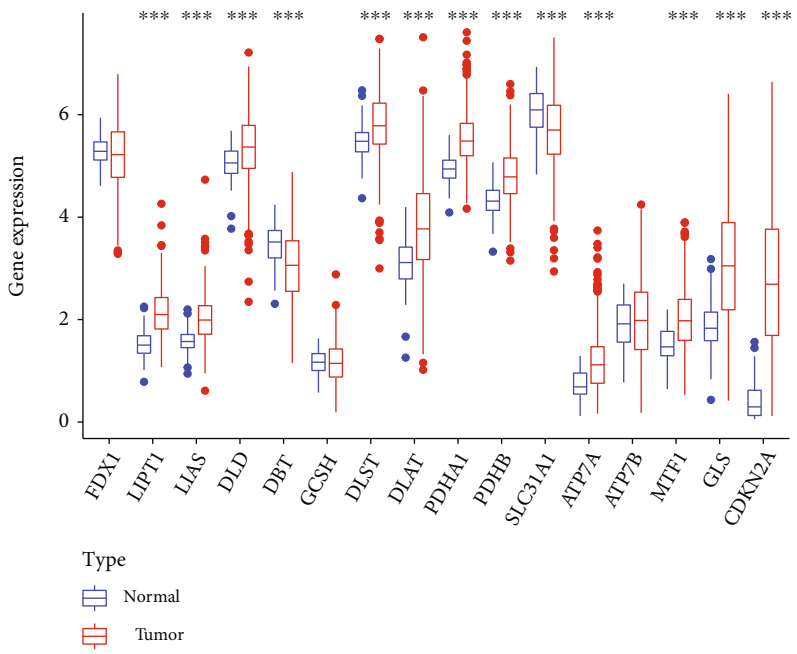

(a)

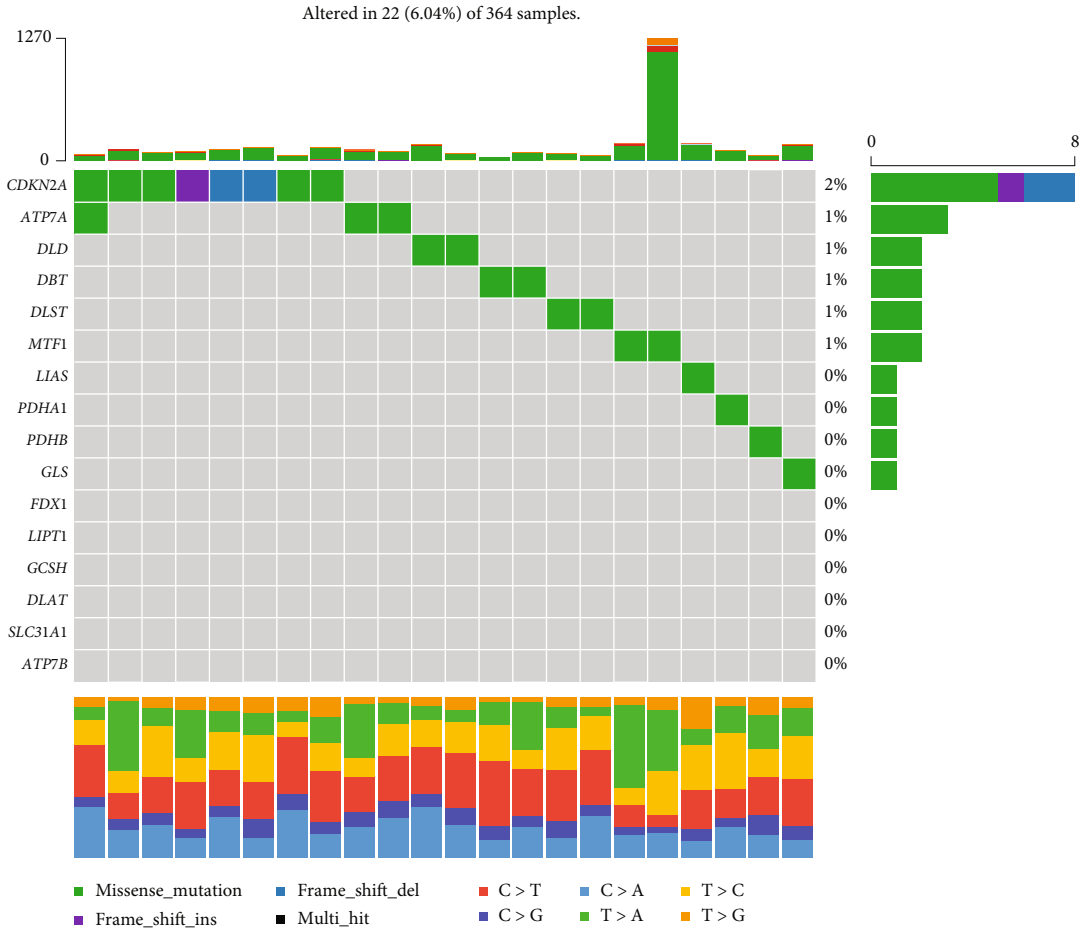

(b)

Figure 2: Continued.

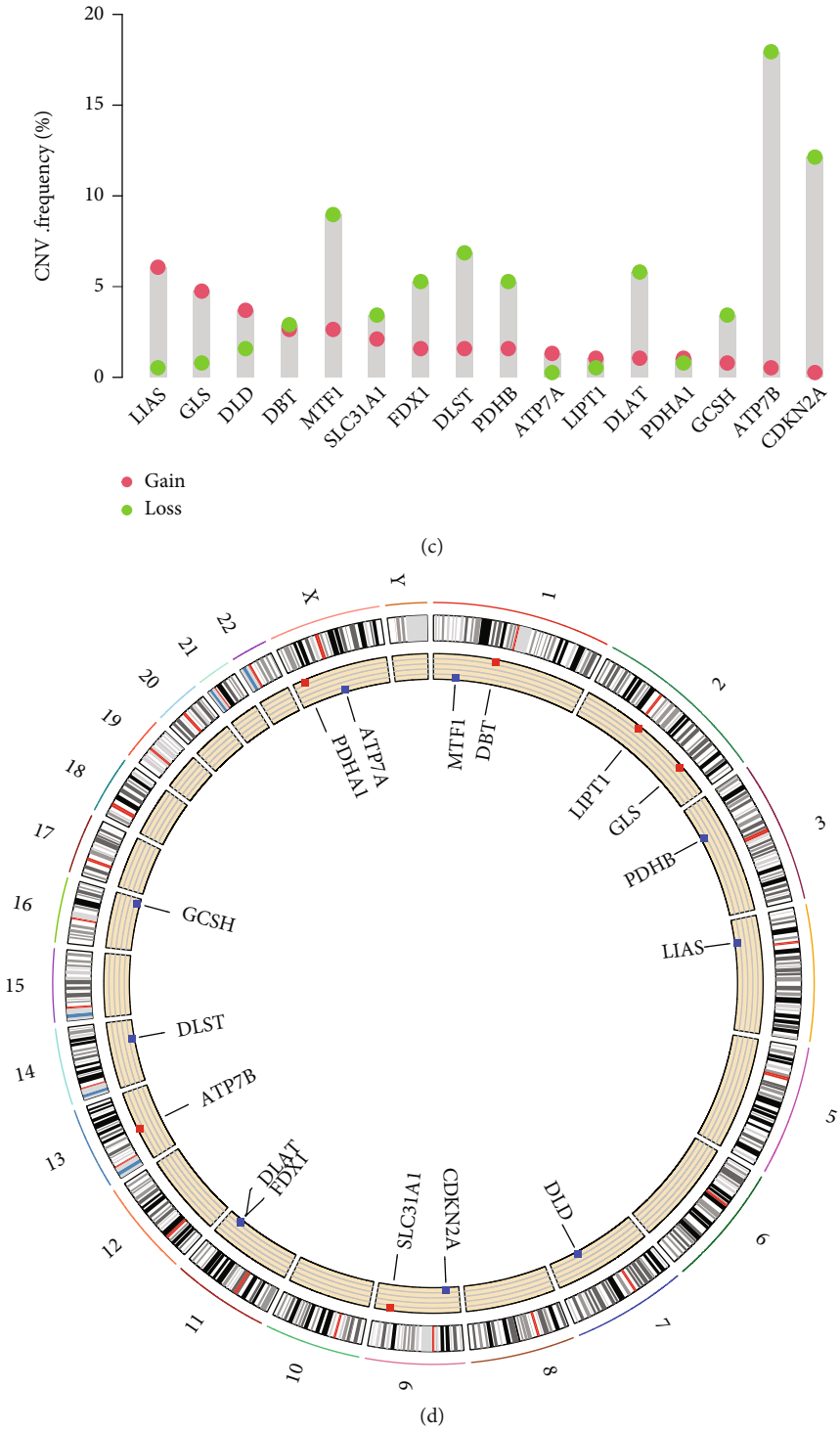

Figure 2: Molecular characterization of CRGs in HCC. (a) Differential expression of CRGs between normal and tumor samples. (b) Waterfall map of CRG mutation. (c) CNA frequency of CRGs. (d) Circos plot of detected CNVs in CRGs. *** represents $p < 0.001$.

SLC31A1, and ATP7B are significantly higher expressed in C2, while ATP7A, MTF1, GLS, and CDKN2A are the opposite (Figure 4(d)). According to these findings, the two molecular subtypes behave differently in cuproptosis.

3.2.2. Differentially Enriched GSVA Function between the Molecular Subtypes. The GSVA analysis shows the activation of KEGG pathways in C1/C2 HCC samples. Metabolism-related pathways such as fatty acid metabolism and drug metabolism, gene stability-related pathways such as DNA replication and mismatch repair, cell cycle, and citrate cycle tricarboxylic acid (TCA) cycle are significantly enriched (Figure 5(a) and Supplementary Table 1). The disorder of TCA cycle caused by excess copper directly result in the

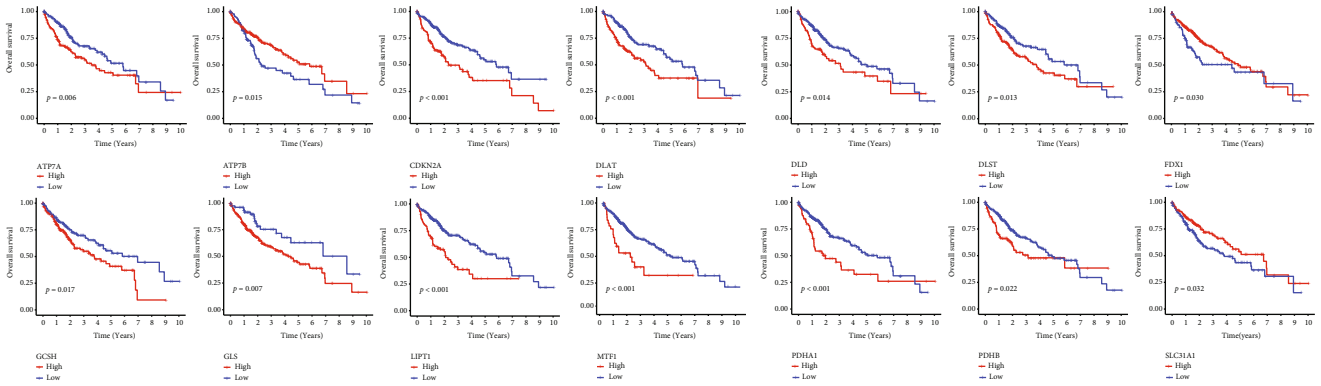

(a)

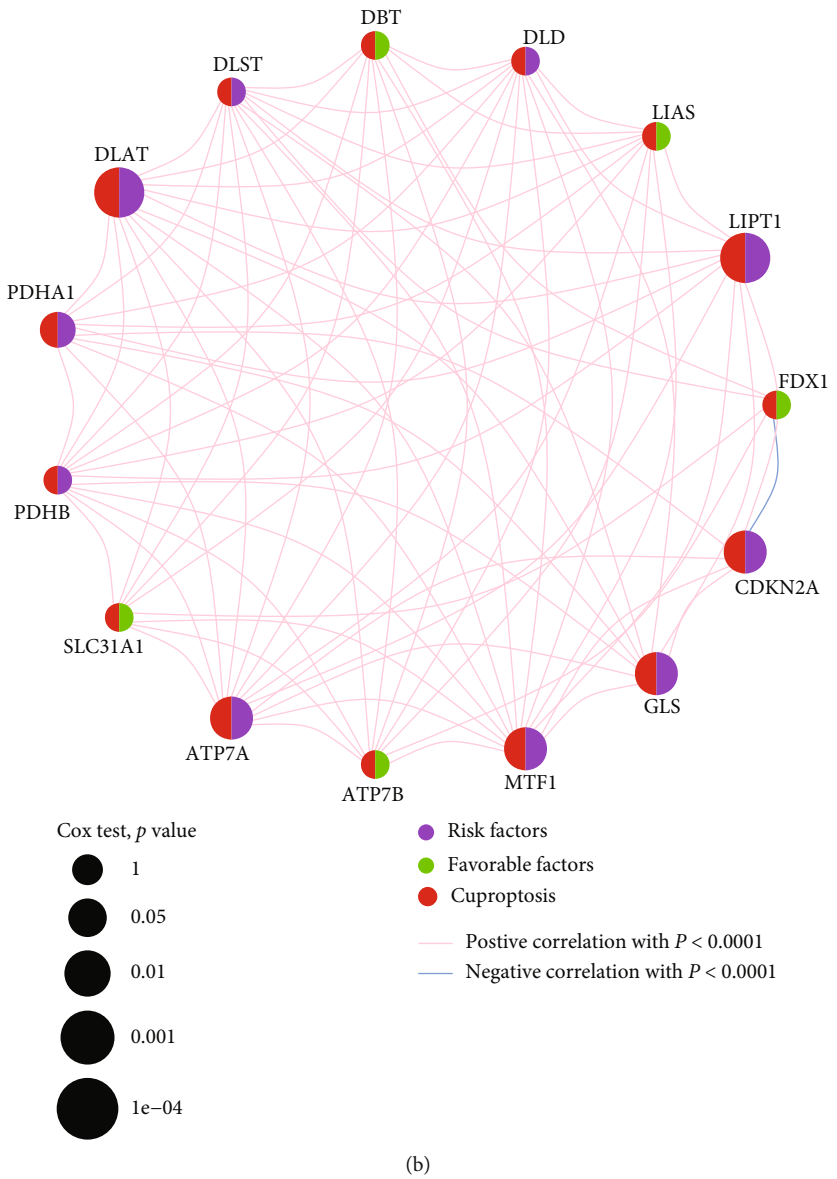

(b)

Figure 3: Continued.

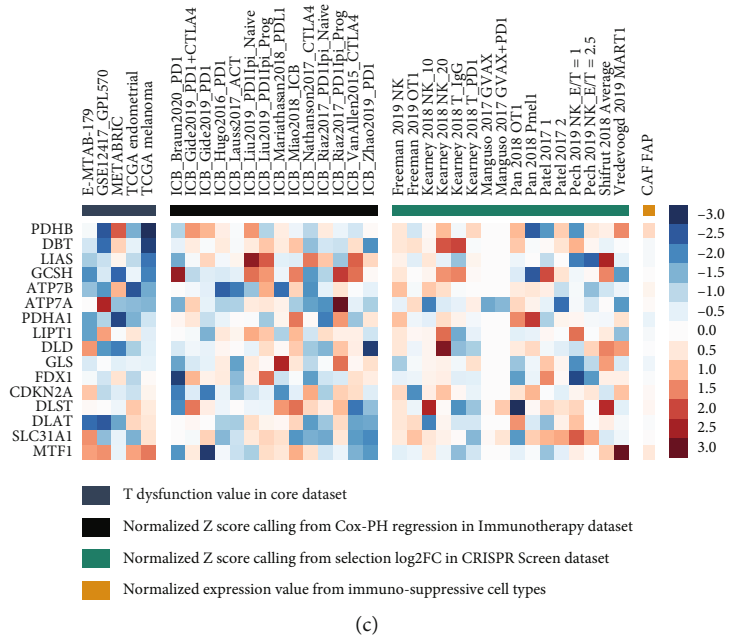

(c)

Figure 3: Survival and immune characterization of CRGs in HCC. (a) The K-M plots of CRGs associated with prognosis. (b) Correlation network of CRGs. (c) TIDE analysis of CRG set.

occurrence of cuproptosis, and the significantly enriched TCA cycle pathway indeed proves the rationale of the molecular subtype.

3.2.3. Comparison of Immune Checkpoint Genes, Immune Cells, and Immune Score Levels between the Molecular Subtypes. Immune checkpoint genes including PDCD1, CD274, CTLA4, TIGIT, LAG3, and LGALS9 are significantly expressed lower in C2 (Figure 5(b)). The results of ssGSEA analysis show that the activated $CD4^+$ T cell, $CD56^{dim}$ natural killer cell, eosinophil, MDSC, type 2 T helper cell, type 1 T helper cell, and type 17 T helper cell are differentially infiltrated between the molecular subtypes (Figure 5(c)). A total of 3 kinds of immune response, including APC costimulation, HLA, and type II IFN response are differentially enriched between the subtypes (Figure 5(c)). The exclusion score is significantly lower in C2, while the dysfunction score and the integrated TIDE score do not present differences between molecular subgroups (Figure 5(d)). Moreover, the StromalScore of C2 is higher than C1, while the ImmuneScore is the opposite (Figure 5(e)). These results suggest that the tumor microenvironment driven by cuproptosis of the two molecular subtypes is diverse from each other.

3.3. Construction and Validation of CRG-Related Signature

3.3.1. A CRG-Related Signature with Independent Prognostic Effect Was Constructed. A 6-gene signature was constructed based on the 1479 DEGs between molecular subtypes with univariate Cox regression analysis and LASSO regression analysis (Figures 6(a)–6(d)). Multivariate Cox regression analysis of the 6 genes shows that MIR1244-2, CBX2, CLEC3B, and SLC16A11 are independent prognostic factors (Figure 6(e)). The cutoff point was set as 1.570 according to the AIC (Figure 6(f)). The AUC of 1-, 2-, and 3-year is 0.775, 0.768, and 0.757, respectively (Figure 6(g)), and the 1-year ROC was further compared with age (AUC = 0.534), gender (AUC = 0.513), histologic grade (AUC = 0.505), and TNM stage (AUC = 0.664) (Figure 6(h)).

HCC samples were divided into high- and low-risk groups in accordance with the AIC value. The overall survival of patients in low-risk group is superior to these in high-risk (Figures 7(a)–7(c)). The univariate Cox regression analysis indicates that the risk status ($p < 0.001$, HR = 1.478, and 95%CI [1.350 – 1.619]) and TNM stage ($p < 0.001$, HR = 1.680, and 95%CI [1.369 – 2.062]) are the risk factors for HCC patients, and the multivariate Cox regression analysis further proved that the risk score ($p < 0.001$, HR = 1.418, and 95%CI [1.279 – 1.572]) acts as an independent role (Figures 7(d) and 7(e)). There is no difference between age and gender in the distribution of risk scores, while increased risk scores are associated with worse histologic grade and more advanced TNM stage (Figures 7(f)–7(i)). CRGs including FDX1, DBT, GCSH, DLST, SLC31A1, and ATP7B are significantly highly expressed in the low-risk group, while LIPT1, DLAT, PDHA1, ATP7A, MTF1, GLS, and CDKN2A are the opposite (Figure 7(j)). Thus, the CRG-related signature represents an eligible AUC value as an independent prognostic factor and it is superior to other clinical phenotypes. The differential expression of CRGs between the two groups suggests that they perform differently on cuproptosis.

3.3.2. Differentially Enriched GSVA Function between the Risk Groups. The results of GSVA analysis present the differentially enriched KEGG pathways in low-risk/high-risk HCC samples. Immune-related pathways such as T cell receptor signaling pathway and B cell receptor signaling

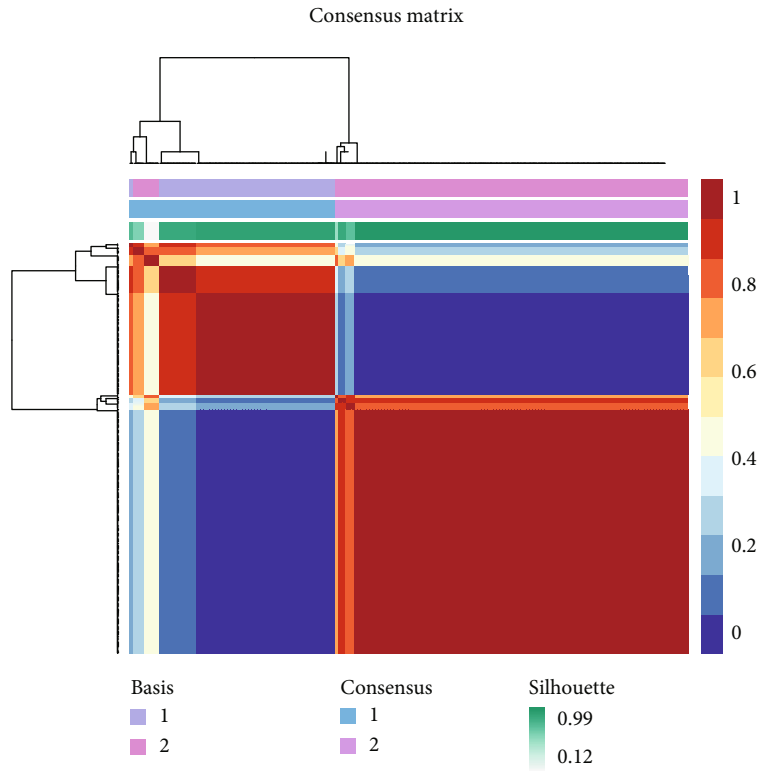

(a)

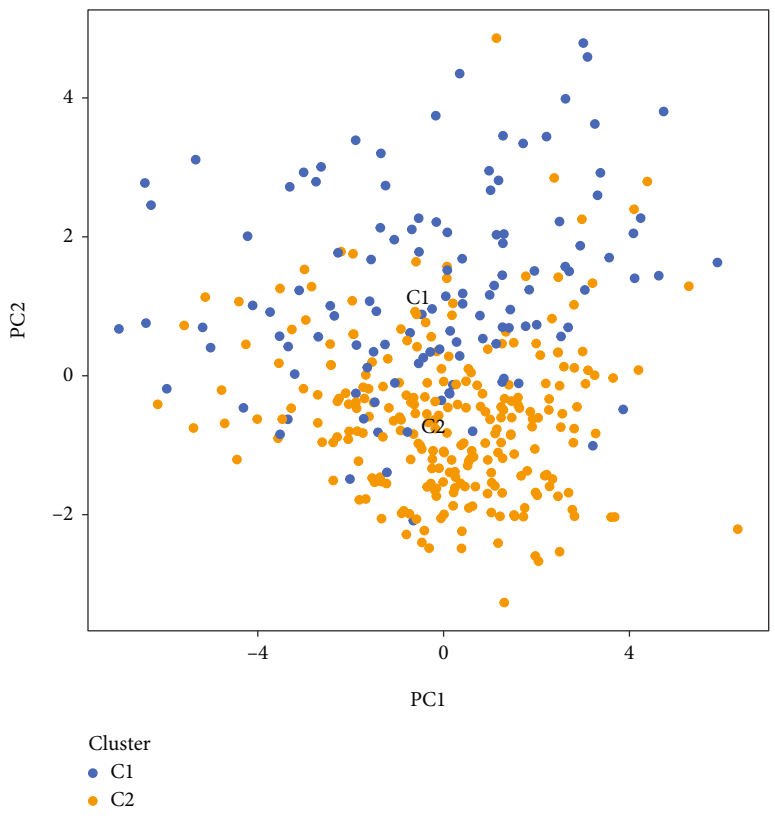

(b)

Figure 4: Continued.

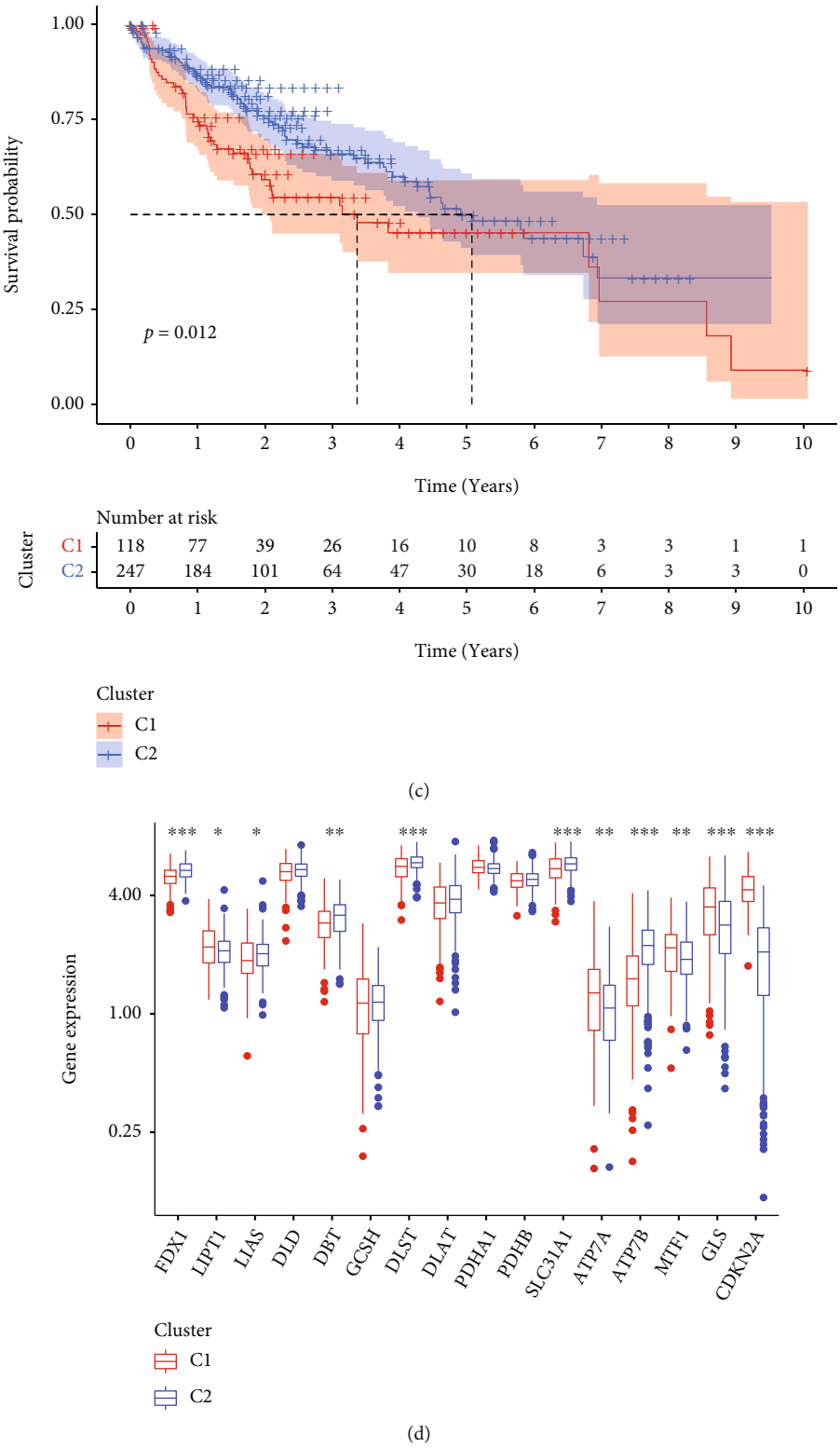

Figure 4: Construction and validation of the cuproptosis-related molecular subtype. (a) Consensus matrix of NMF analysis. (b) PCA analysis of the molecular subtype. (c) The K-M plot of the molecular subtype. (d) Differential expression of CRGs between molecular types. *represents $p < 0.05$, **represents $p < 0.01$, and ***represents $p < 0.001$.

pathway, gene stability-related pathways such as DNA replication and mismatch repair, cell cycle, and citrate cycle TCA cycle are significantly enriched (Figure 7(k) and Supplementary Table 2). It is apparent from these data that the signature inherits the molecular characteristics of the molecular subtype.

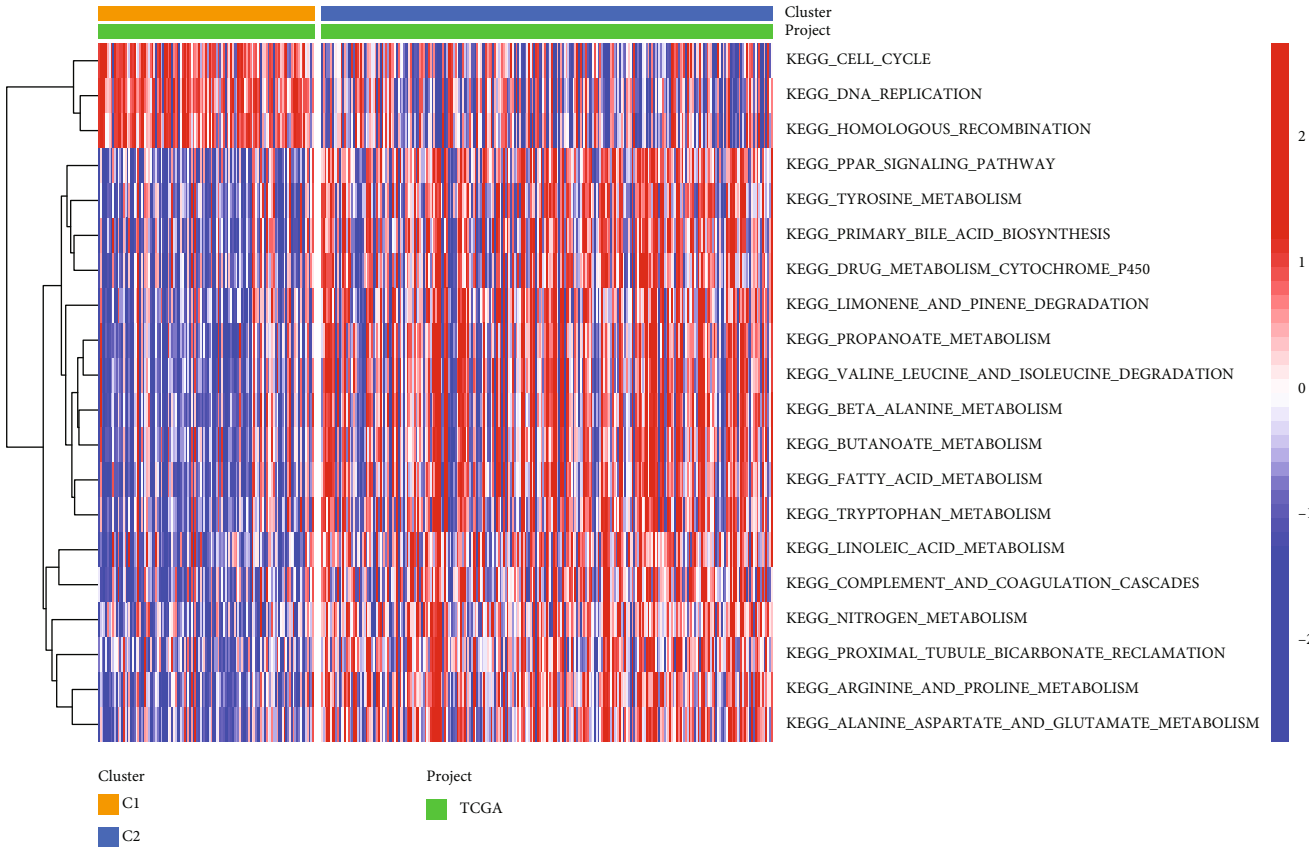

(a)

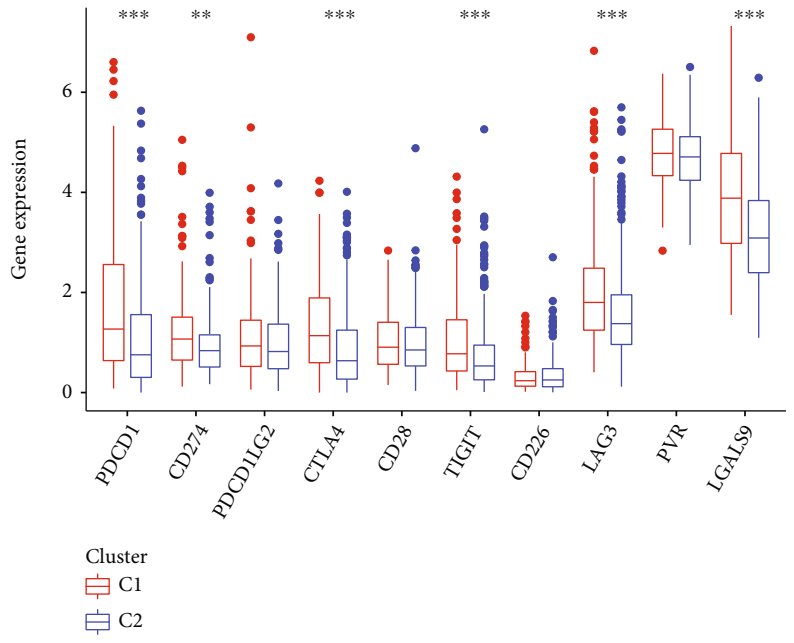

(b)

Figure 5: Continued.

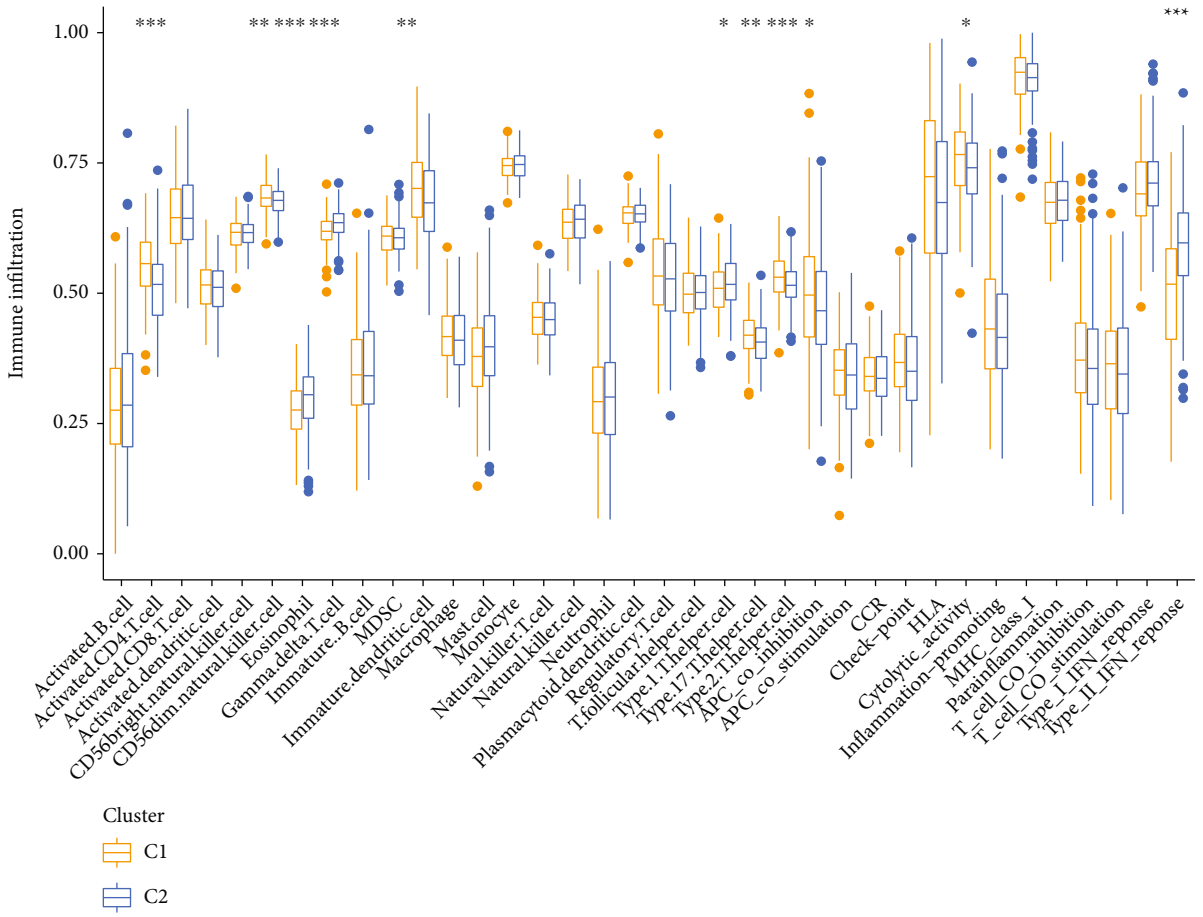

(c)

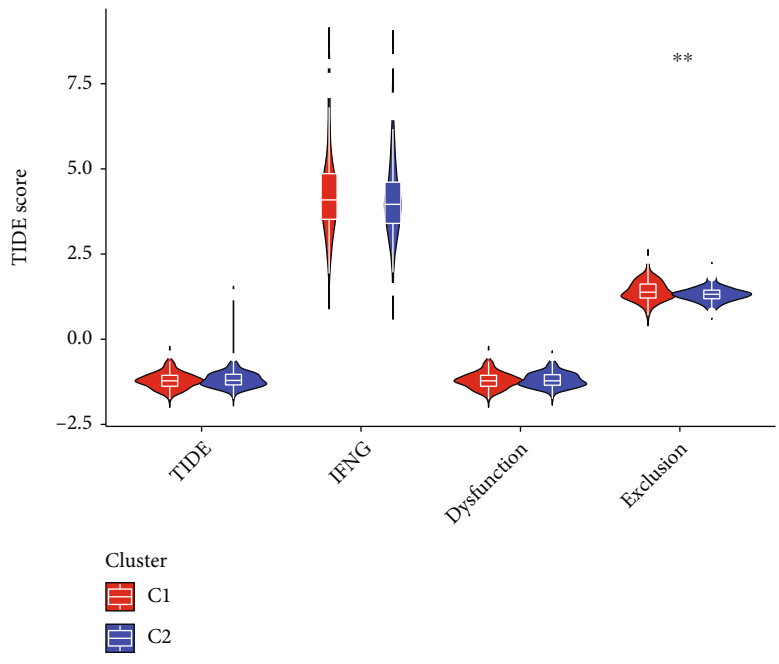

(d)

Figure 5: Continued.

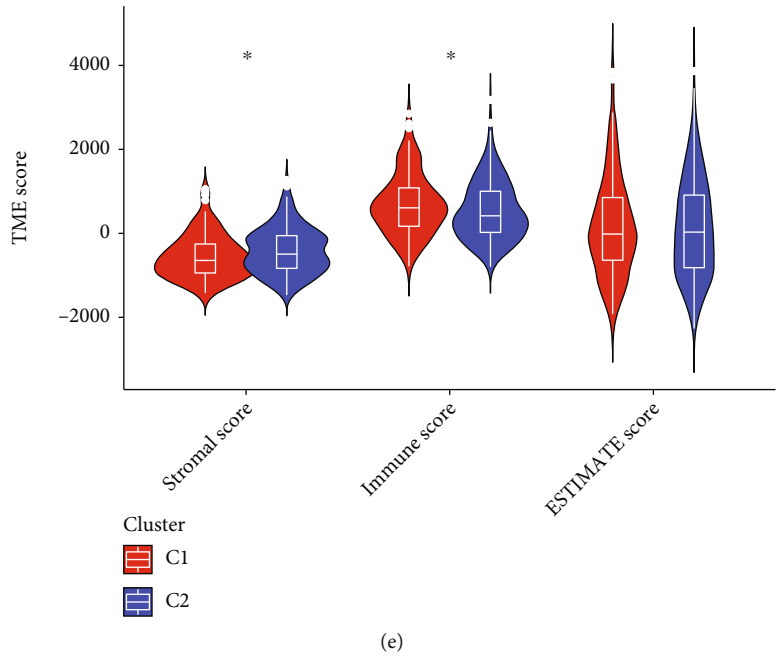

(e)

Figure 5: Function enrichment and immune landscape of the cuproptosis-related molecular subtype. (a) GSVA heat map of the molecular subtype. (b) Differential expression of immune checkpoint genes between molecular types. (c) ssGSEA analysis of the molecular subtype. (d) TIDE score of the molecular subtype. (e) Immune-stromal component evaluation of the molecular subtype. * represents $p < 0.05$, ** represents $p < 0.01$, and *** represents $p < 0.001$.

3.3.3. Comparison of Immune Checkpoint Genes, Immune Cells, and Immune Score Levels between the Two Risk Groups. The results of ssGSEA analysis show that the activated $CD4^+$ T cell, activated dendritic cell, eosinophil, gamma-delta T cell, MDCS, regulatory T cell, type 1 T helper cell, and type 2 T helper cell are differentially infiltrated between the risk groups (Figure 8(a)). Immune functions including APC costimulation, HLA, MHC class I, type I IFN response, and type I IFN response are differentially enriched between the risk groups (Figure 8(a)). Immune checkpoint genes including PDCD1, CTLA4, TIGIT, LAG3, PVR, and LGALS9 are significantly expressed lower in the low-risk group (Figure 8(b)).

Correlations between risk scores and tumor-infiltrating immune cells are presented in Figure 8(c) and Supplementary Table 3. The risk score is strongly and negatively related to the infiltration level of endothelial cell, hematopoietic stem cell, macrophage M2, while positively correlated to T cell CD4+ Th2, neutrophil, macrophage, myeloid dendritic cell, macrophage M1, monocyte, T cell regulatory, and NK cell. The exclusion score is significantly higher in the low-risk group, while the dysfunction score and the integrated TIDE score are the opposite (Figure 8(d)). The StromalScore of the high-risk group was lower than the low-risk group, while ImmuneScore was the opposite (Figure 8(e)). Moreover, the risk score is positively related to the TMB score (Figures 8(f) and 8(g)). The tumor microenvironment driven by cuproptosis of the two risk groups differs from each other, which indicates that the signature can be used to predict the immune status of patients with HCC.

3.3.4. Predicting the IC_{50} of Anti-HCC Agents. Figures 9(a)–9(d) present the comparison of IC_{50} for sorafenib, cisplatin, paclitaxel, and gemcitabine between the low- and high-risk groups. The results show that HCC patients in the low-risk group have a higher IC_{50} in the four comparisons, which indicates that the patients in the high-risk group have a tendency to benefit more from the conventional agents. What stands out in this section is that the signature is able to recognize HCC patients who could benefit from conventional anti-HCC drugs.

3.3.5. Correlations between Molecular Subtype and Signature. As shown in Figure 9(e), the risk score level in C1 is significantly higher than in C2. The distribution of patients by molecular subtype, risk score, and survival status are represented in Figure 9(f).

3.3.6. The Signature Was Validated in the LIRI-JP and IMvigor210 Cohort. HCC patients in the LIRI-JP cohort were divided into low- and high-risk groups based on the previously constructed signature. The prognosis of patients in the low-risk group is superior to that of those in the high-risk group (Figure 10(a)). The AUC values of the 1-, 2-, and 3-year ROC curves are 0.811, 0.741, and 0.775, respectively (Figure 10(b)). Tumor patients who positively respond to ICIs have relatively higher risk scores, and tumor patients in the high-risk group are more likely to benefit from ICIs (Figures 10(c) and 10(d)). In summary, for the informants in this section, the signature is robust in predicting the prognosis of HCC and has the potential to foresee the response to immunotherapy.

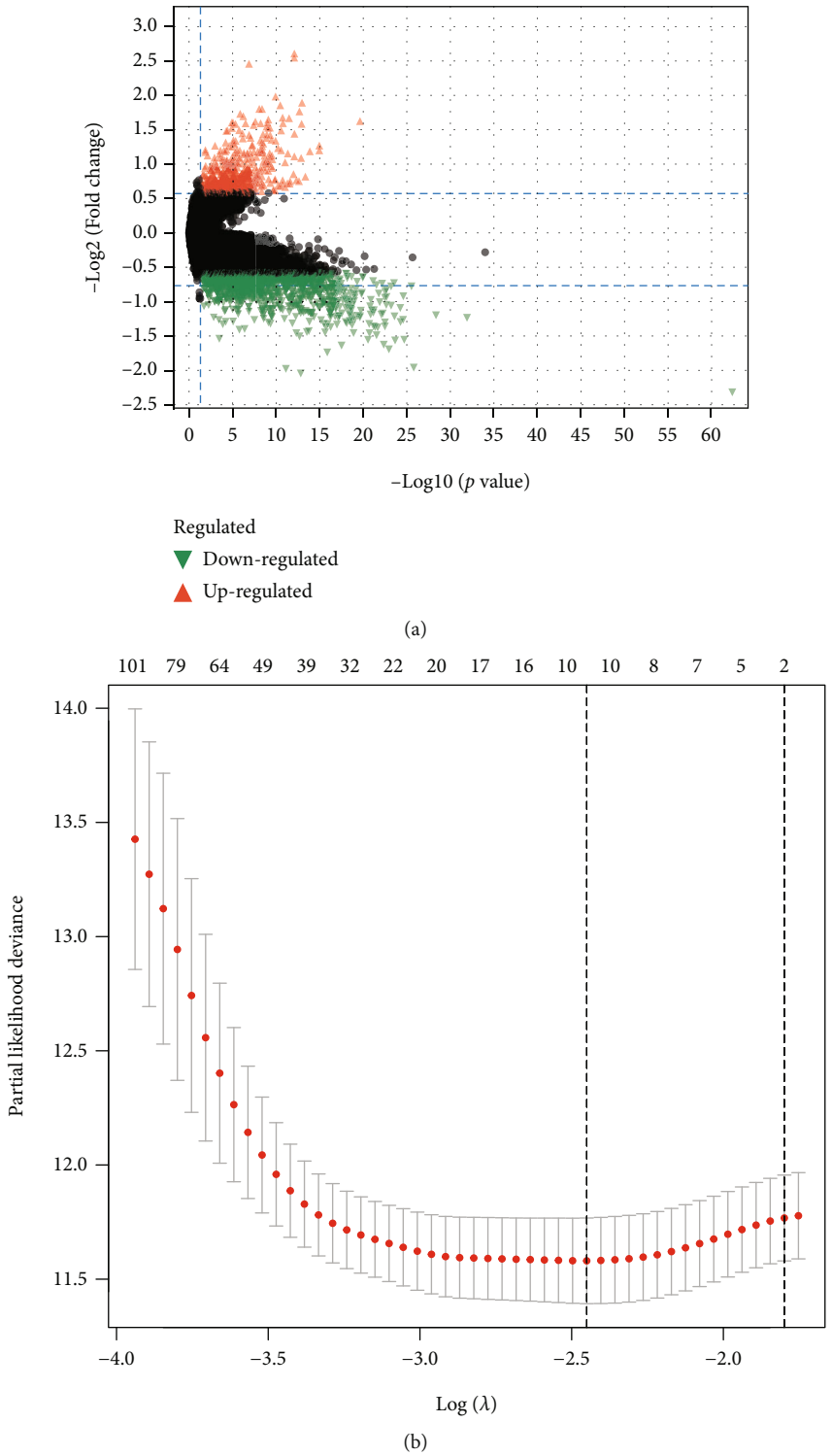

Figure 6: Continued.

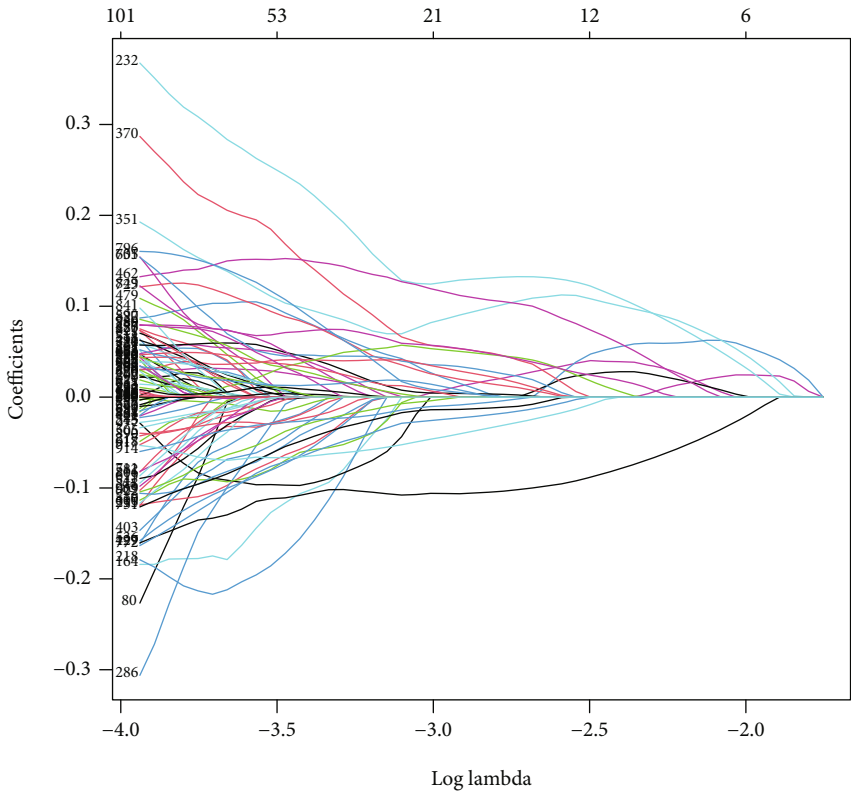

(c)

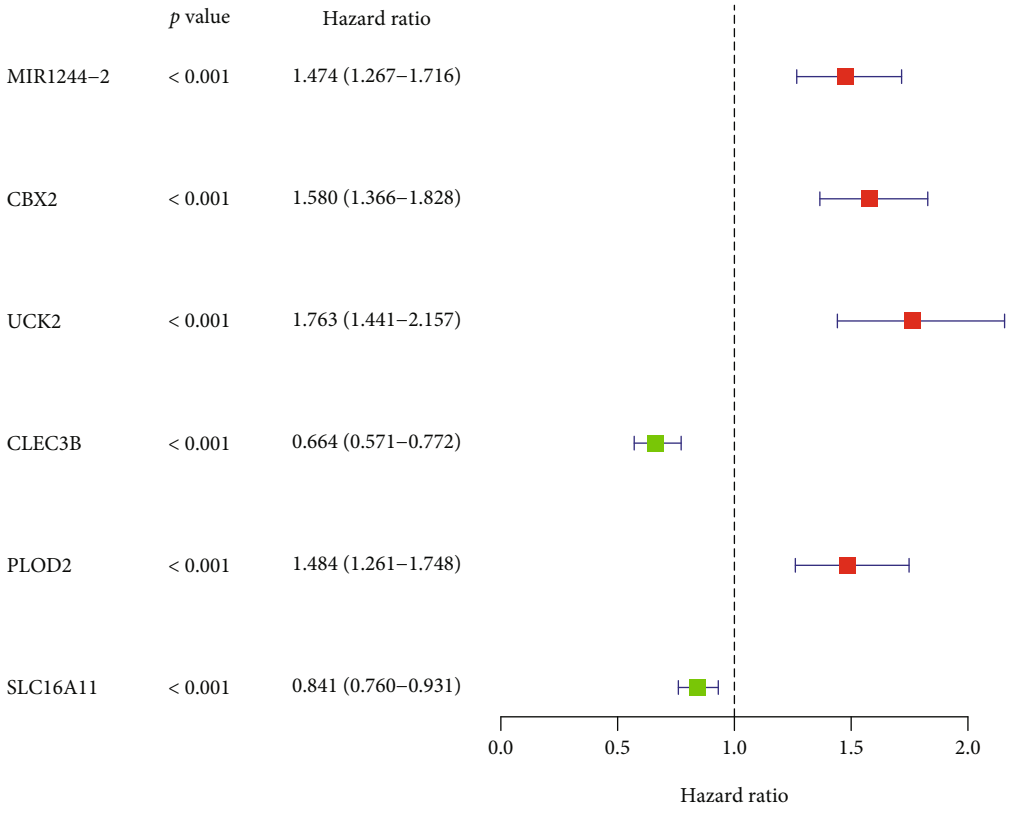

(d)

Figure 6: Continued.

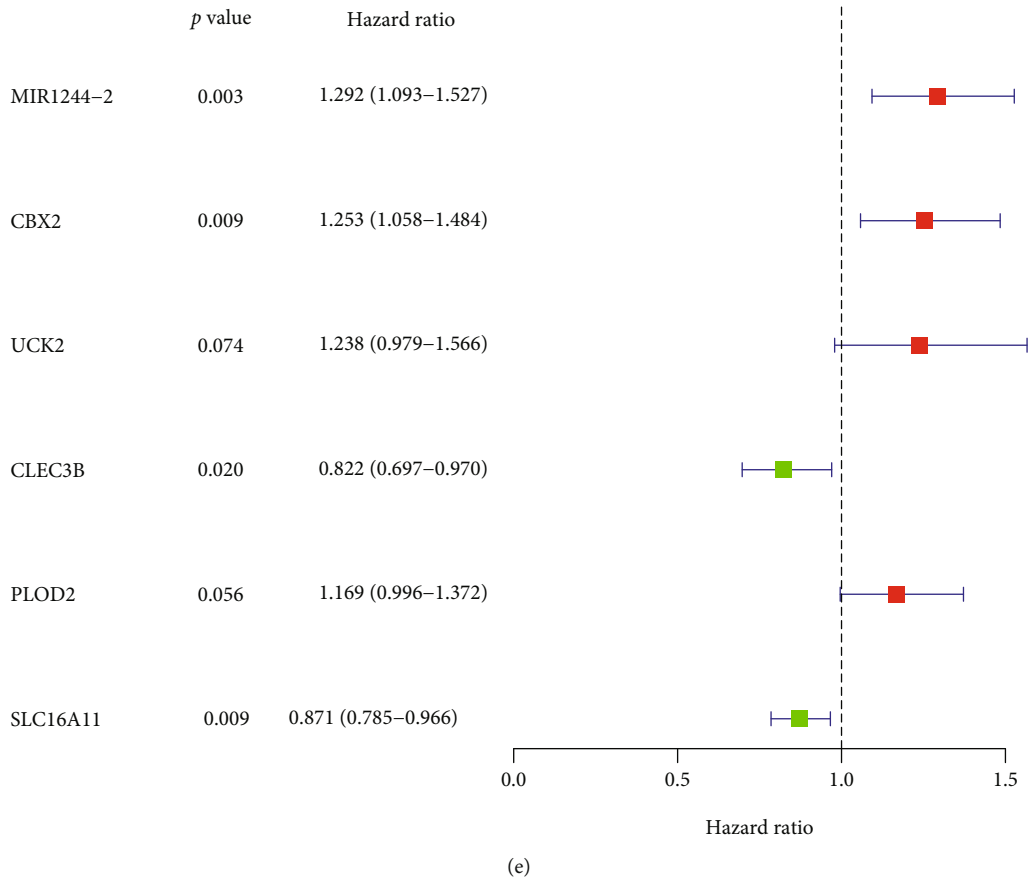

(e)

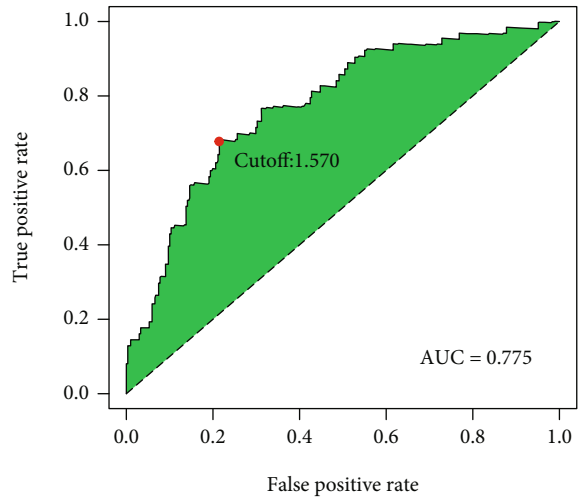

(f)

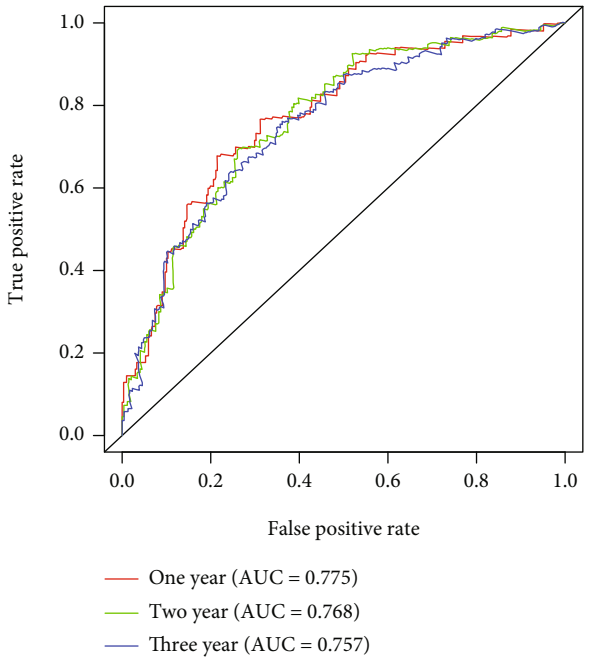

(g)

Figure 6: Continued.

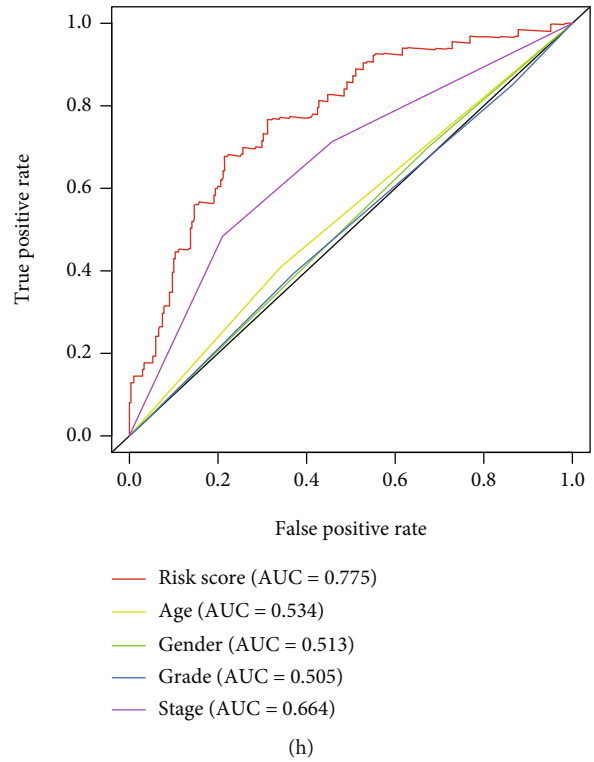

Figure 6: Construction of the cuproptosis-related prognostic signature using the TCGA-LIHC project. (a) Volcano map of the DEGs between molecular subtypes. (b) Distribution of partial likelihood deviation of the LASSO regression. (c) LASSO coefficient profiles. (d) Univariate Cox analysis of the 6 genes in the signature. (e) Multivariate Cox regression analysis of the 6 genes in the signature. (f) Cutoff point used to distinguish the low- and high-risk group. (g) ROC curve for predicting 1-, 2-, and 3-year overall survival. (h) ROC comparison between the signature and tumor stage, histologic grade, age, and gender.

4. Discussion

Cuproptosis was a novel form of regulated cell death proposed by Tsvetkov et al. [15]. It is revealed that the excess intracellular Cu disturbs the mitochondrial TCA cycle, leading to cell death and independent of other cell death pathways [31]. Although the growth inhibition of the elesclomol-Cu complex in HCC-related cell lines was not examined, it has been demonstrated that there is a strong association between Cu metabolism and HCC cell death. Nurmamat et al. synthesized a novel copper (II) complex, which could induce the cell cycle arrest and result in apoptosis in BEL-7404 cells [32]. Cu transporter-related genes such as ATP7A, ATP7B, and SLC31A1 were singularly expressed or copied in liver cancer samples and a relative higher level of Cu was observed in HCC cell [33]. Clinical studies have shown that the high levels of serum copper are associated with poor prognosis in patients with HCC ($p < 0.01$, HR = 2.06, and 95%CI [1.036 – 3.11]) [34]. What is more, Cu propelled the antitumor effects of troxerutin, a rutin derivative, in Huh-7 cells with little toxicity in normal cells [35]. Thus, an abundance of indirect evidence from laboratory to clinical has supported that Cu metabolism is strongly associated with HCC, and targeting CRGs is a potential therapeutic strategy for HCC. A comprehensive bioinformatics analysis of CRGs for molecular subtype identification and prognosis in HCC patients is important.

The molecular characteristic of CRGs in HCC was analyzed in this study. Most of the CRGs were differentially expressed between normal and tumor samples. FDX1 is the key regulator of cuproptosis with the function of inducing protein lipoylation when being deleted, which further results in resistance to cuproptosis [36]. FDX1 is shown to be a favorable factor for HCC patients in our study. Cu transporter-related genes including ATP7A, SLC31A1, and TCA-related genes including DBT, DLST, and DLAT are differentially expressed between normal and tumor samples. The expression of CRGs is associated with their CNV level, which indicates that CNV may contribute the CRGs heterogeneity in HCC. The CNV of Cu transporter-related genes is accompanied by a worse prognosis, which was anteriorly discussed by Davis et al. [33]. GCSH and PDHA1, both involved in protein lipoylation, are predicted to be associated with immunotherapy, however, their concrete role in immunotherapy has not been investigated.

Both molecular subtypes and signatures have significant differences in OS, with C2 superior to C1 and low-risk superior to high-risk. The molecular subtype and signature are strongly associated with cuproptosis, as most of the CRGs are differentially expressed between different molecular subtypes and risk groups. Highly expressed FDX1 and SLC31A1 are steadily associated with better prognosis in HCC patients, while ATP7A, MTF1, GLS, and CDKN2A are the opposite. MTF1, GLS, and CDKN2A were proved to be

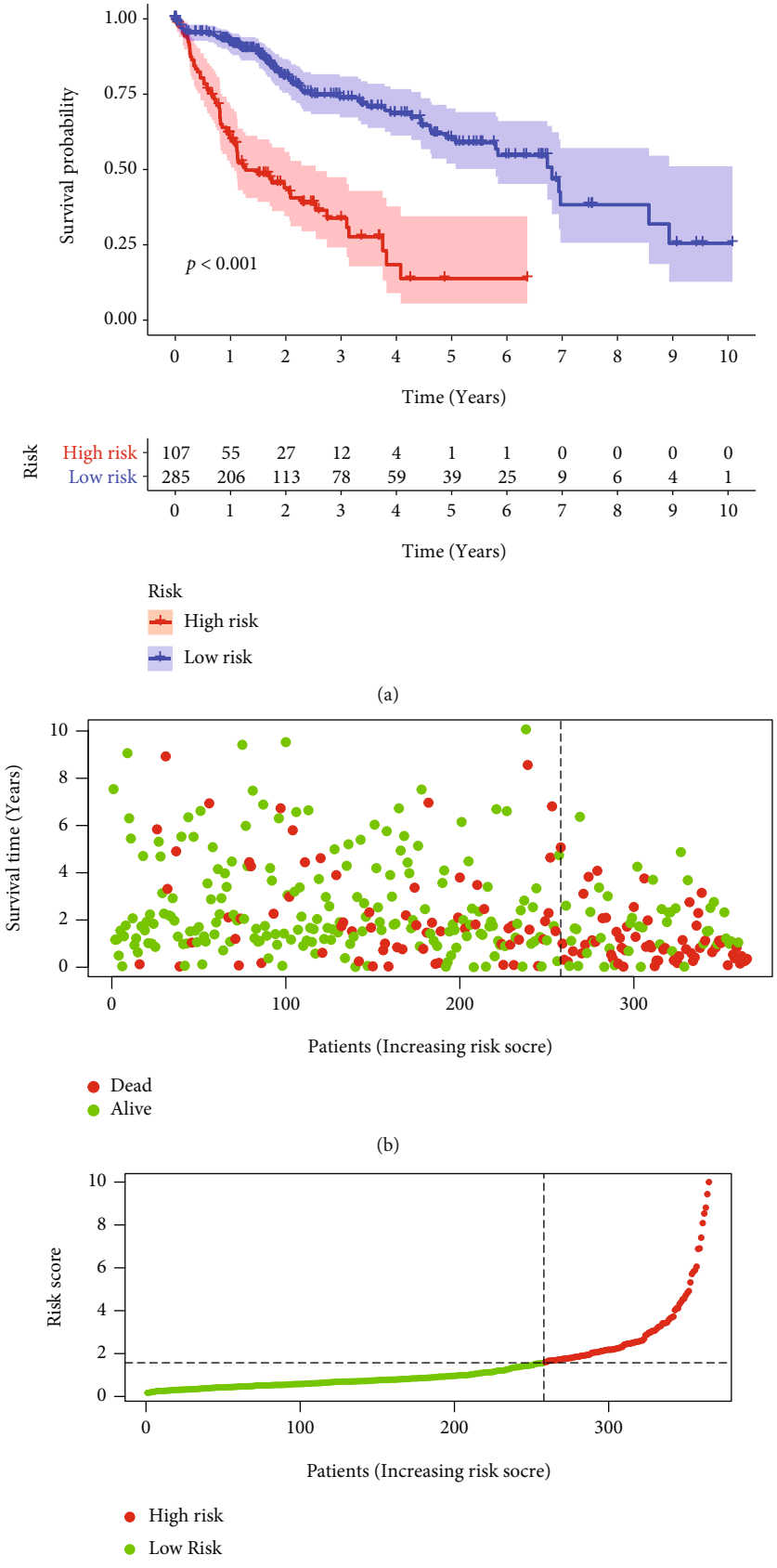

Figure 7: Continued.

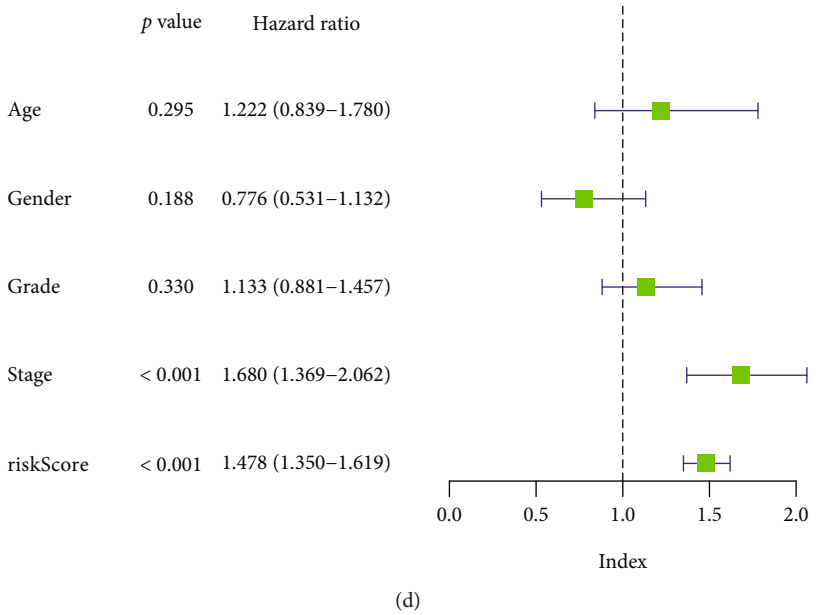

(d)

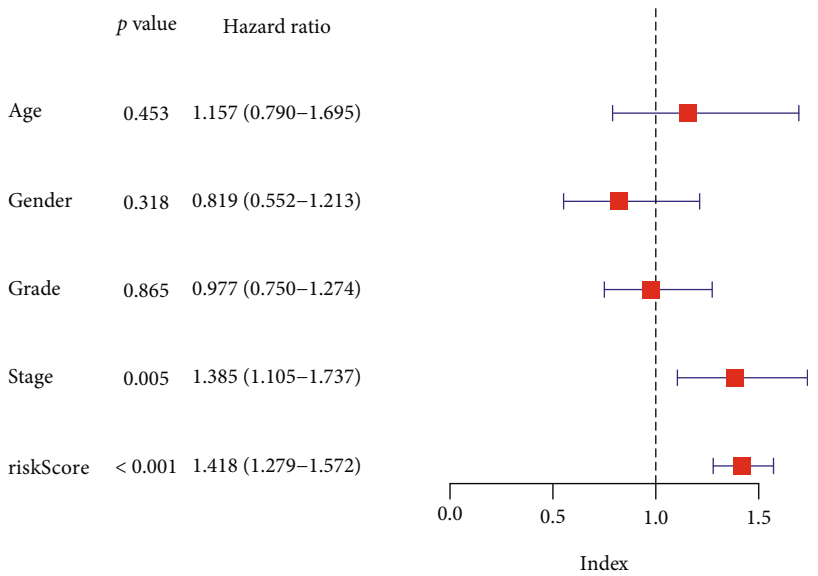

(e)

Figure 7: Continued.

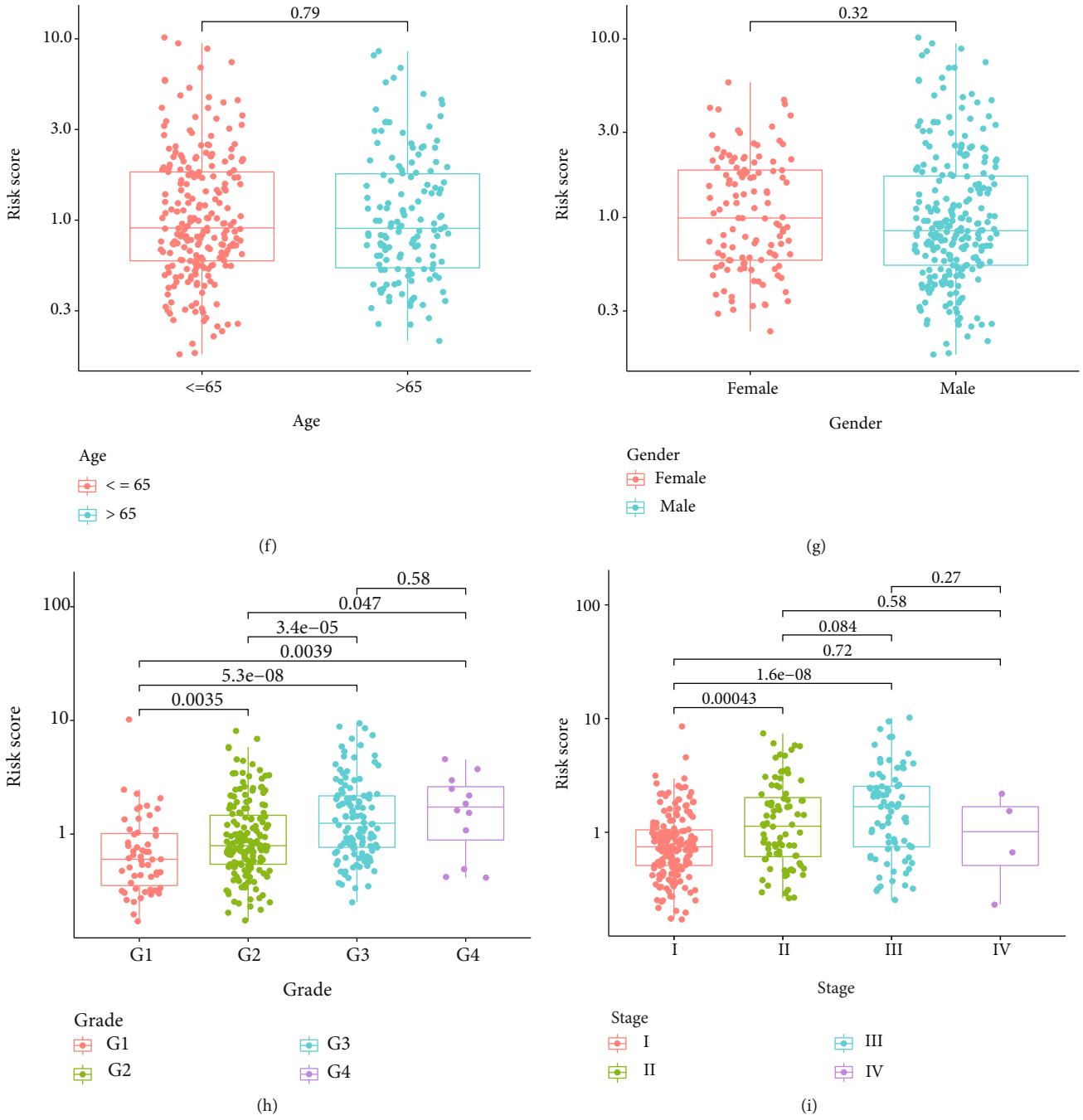

Figure 7: Continued.

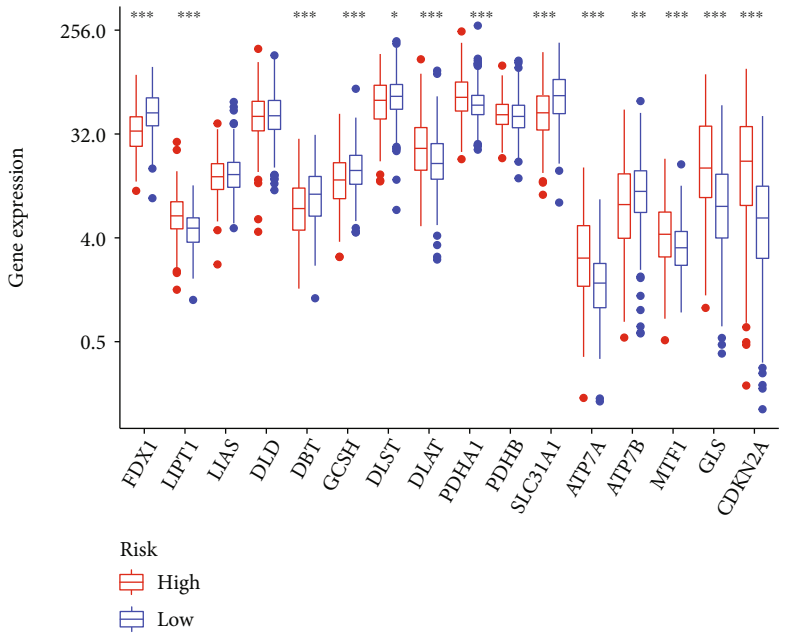

(j)

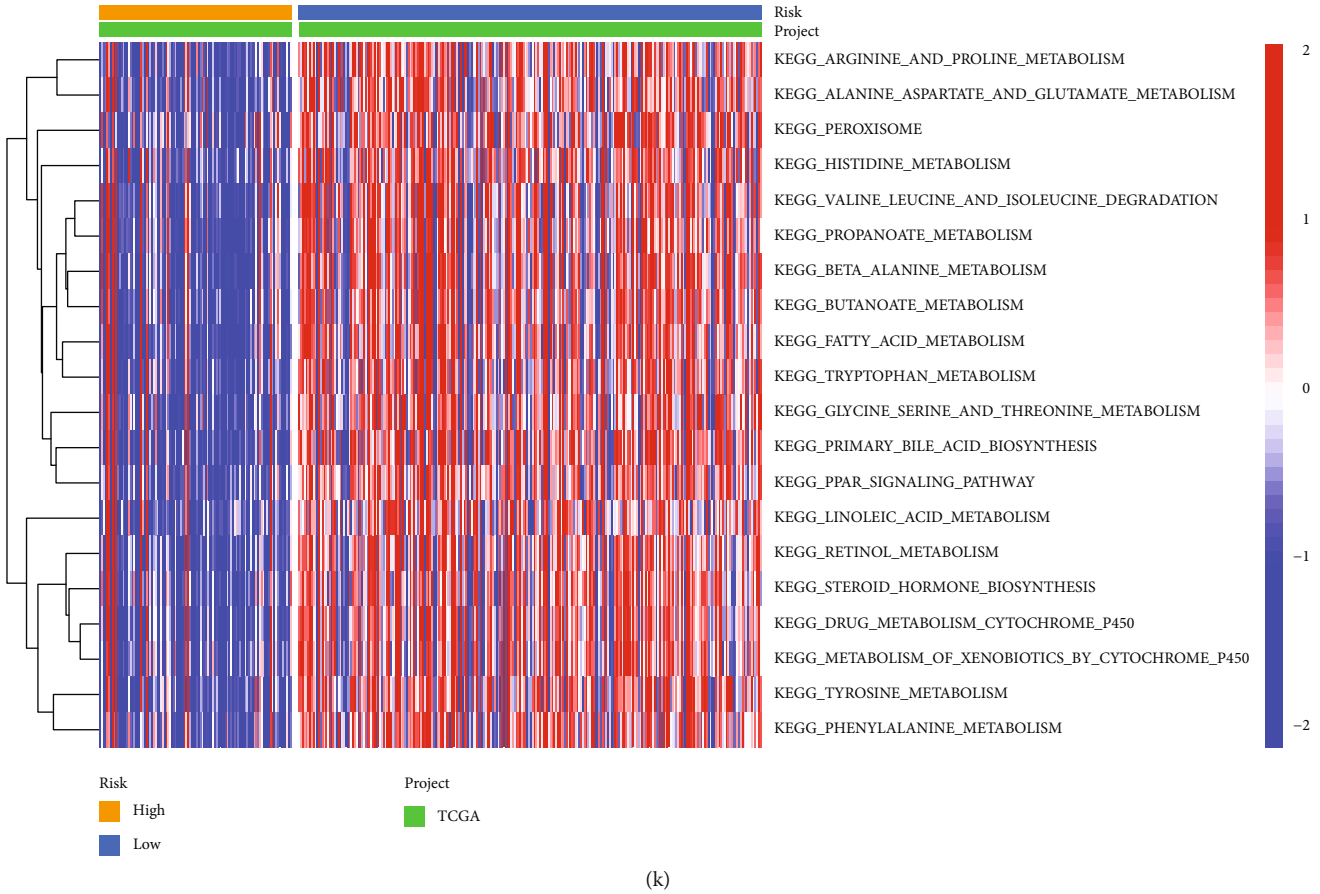

(k)

Figure 7: Validation of the cuproptosis-related prognostic signature in the TCGA-LIHC project. (a) The K-M plot of the signature. (b) Distribution of the survival states. (c) Distribution of the risk scores. (d) Univariate Cox analysis of the signature with clinical phenotypes. (e) Multivariate Cox regression analysis of the signature with clinical phenotypes. (f) Distribution of risk scores by age. (g) Distribution of risk scores by gender. (h) Distribution of risk scores by histologic grade. (i) Distribution of risk scores by tumor stage. (j) Differential expression of CRGs between the low- and the high-risk groups. (k) GSVA heat map of the signature. *represents p <0.05, ** represents $p < 0.01$, and ***represents $p < 0.001$.

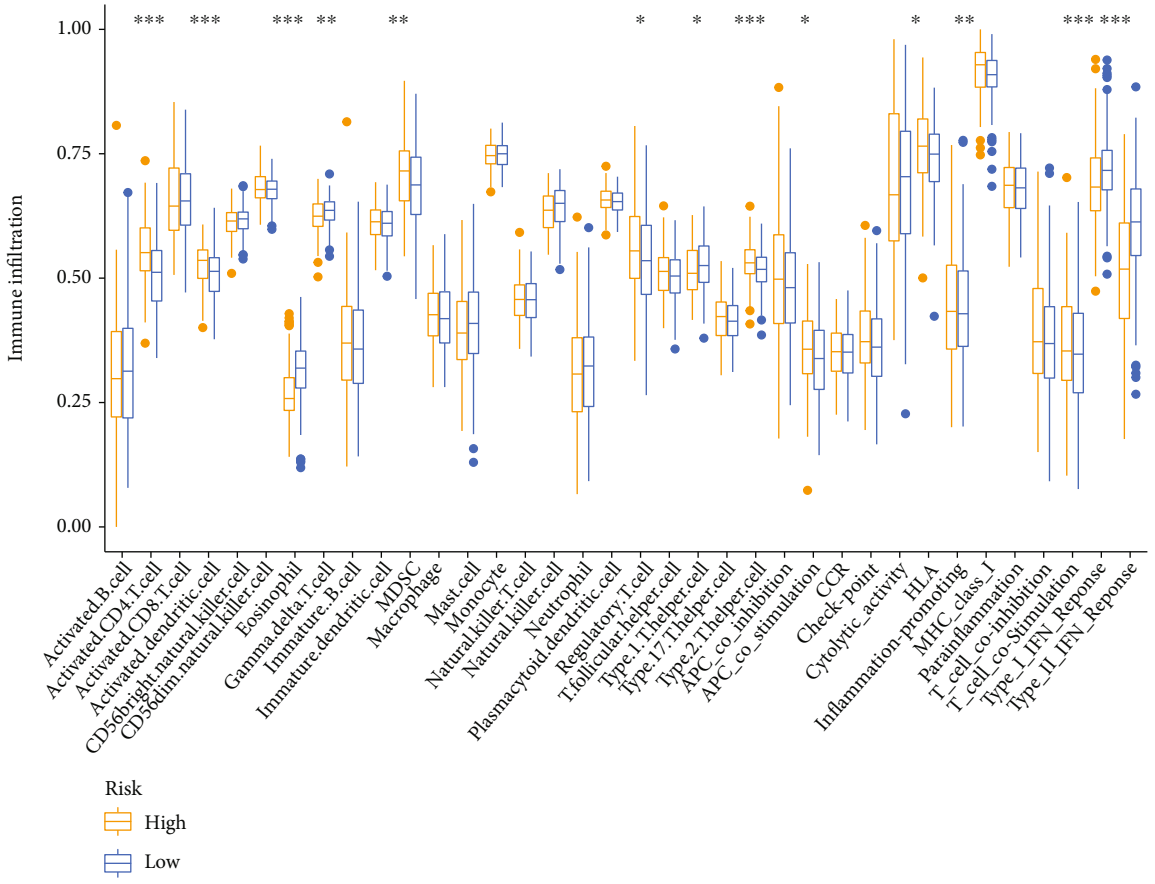

(a)

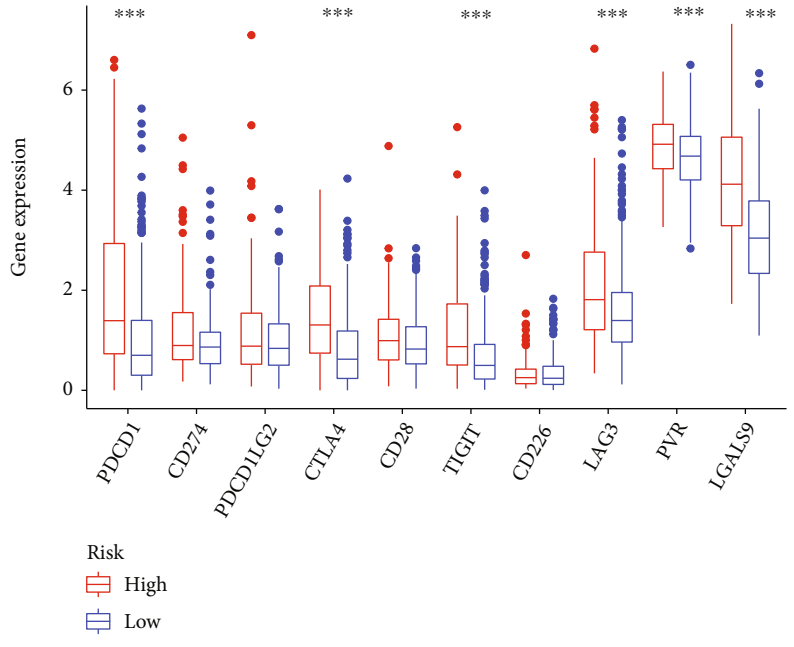

(b)

Figure 8: Continued.

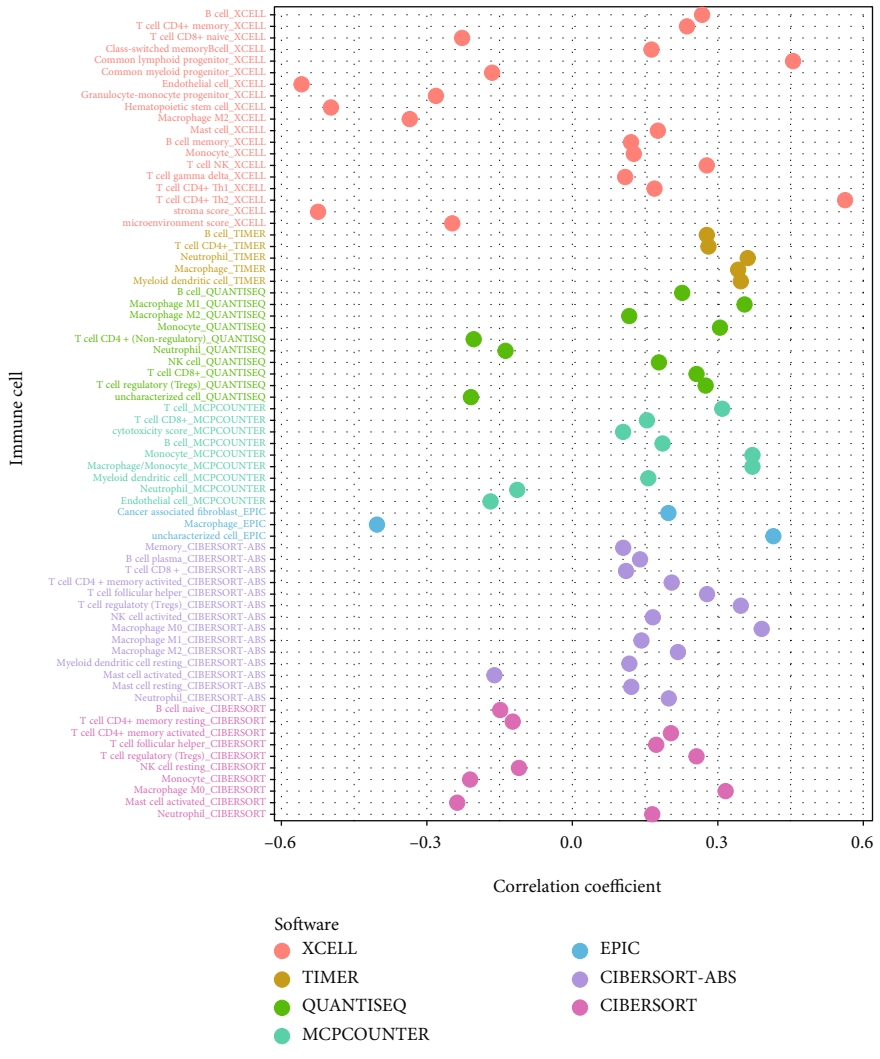

(c)

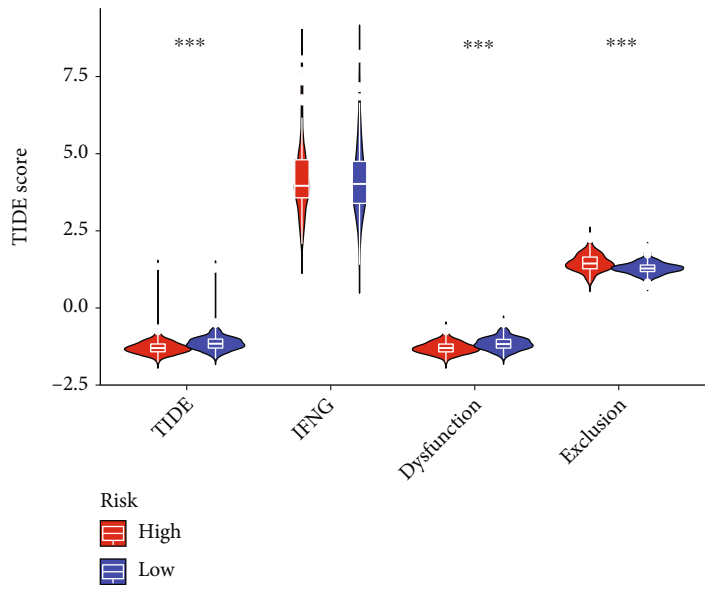

(d)

Figure 8: Continued.

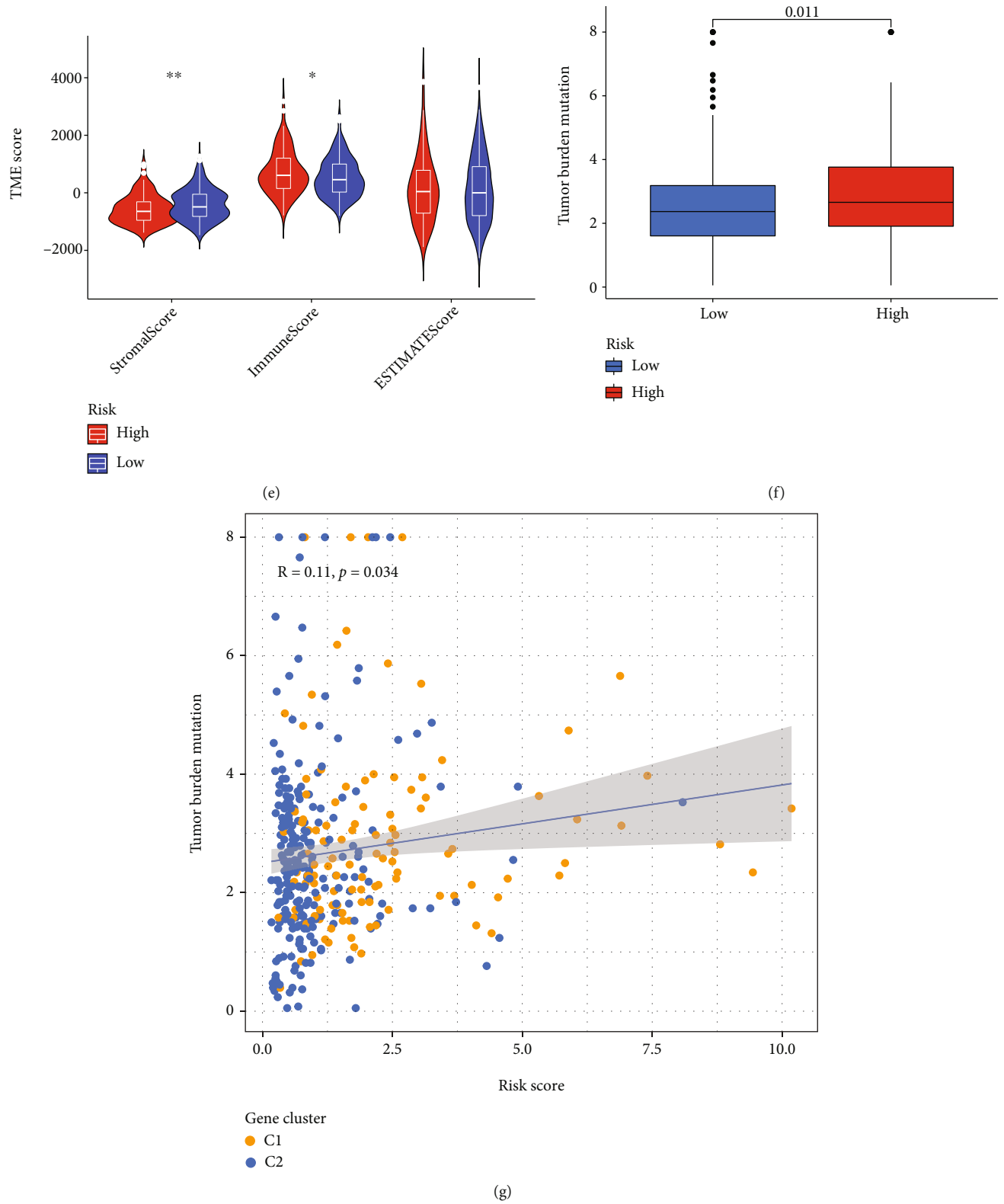

Figure 8: Immune landscape of the cuproptosis-related signature. (a) ssGSEA analysis of the signature. (b) Differential expression of immune checkpoint genes between the low- and high-risk groups. (c) The correlation of tumor-infiltrating immune cells and risk scores based on 7 algorithms. (d) TIDE score of the signature. (e) Immune-stromal component evaluation of the signature. (f) Comparison of TMB levels between the low- and high-risk groups. (g) The correlation between TMB level and risk score. *represents $p < 0.05$, ** represents $p < 0.01$, and ***represents $p < 0.001$.

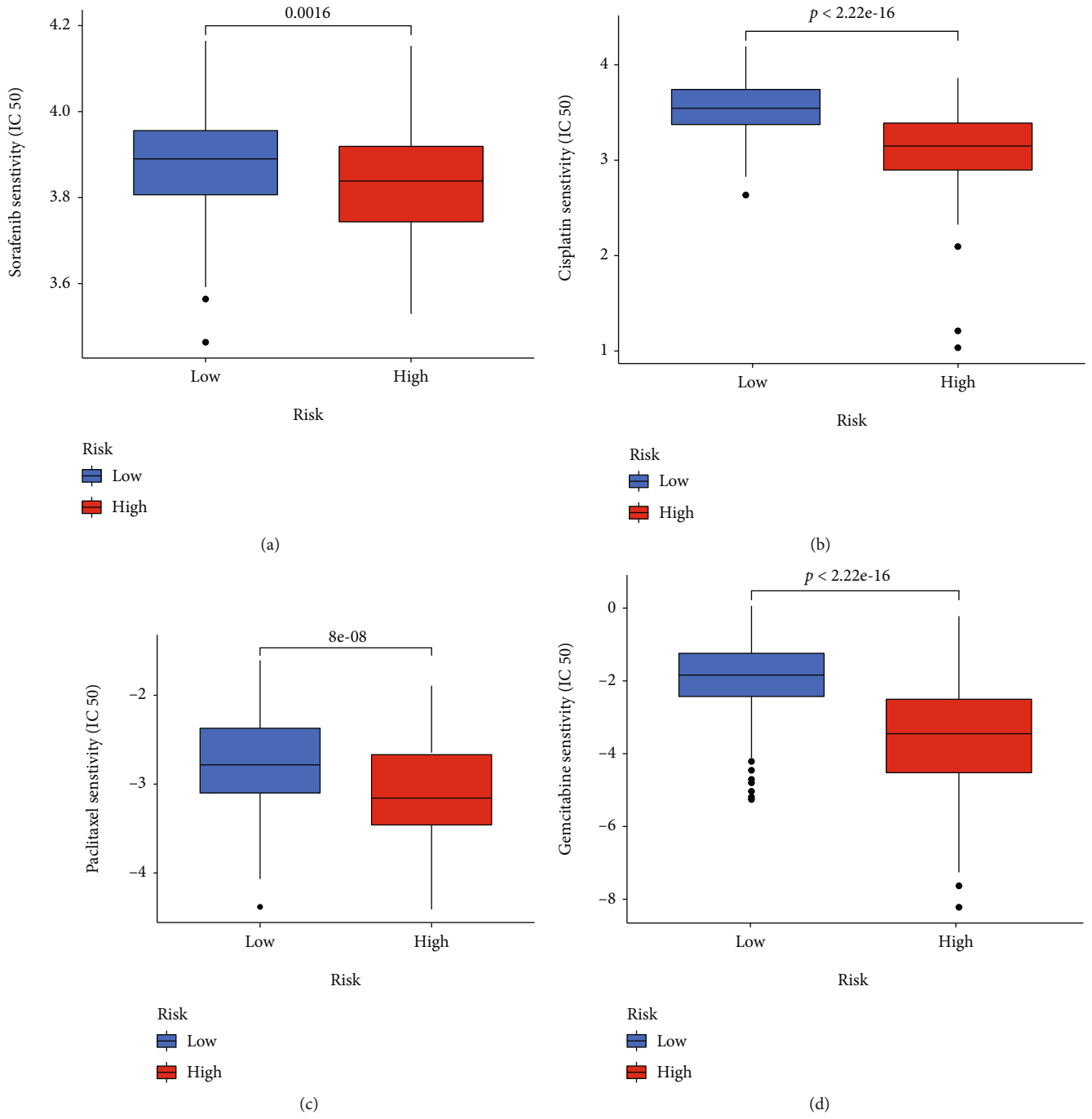

Figure 9: Continued.

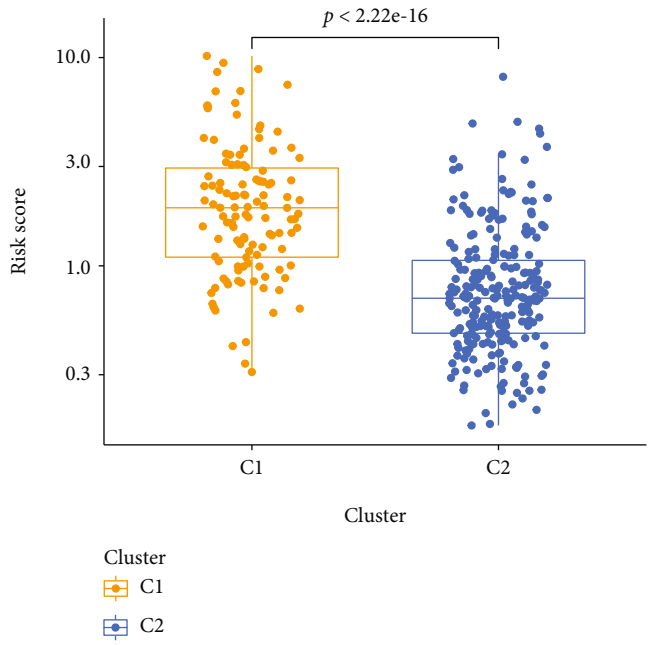

(e)

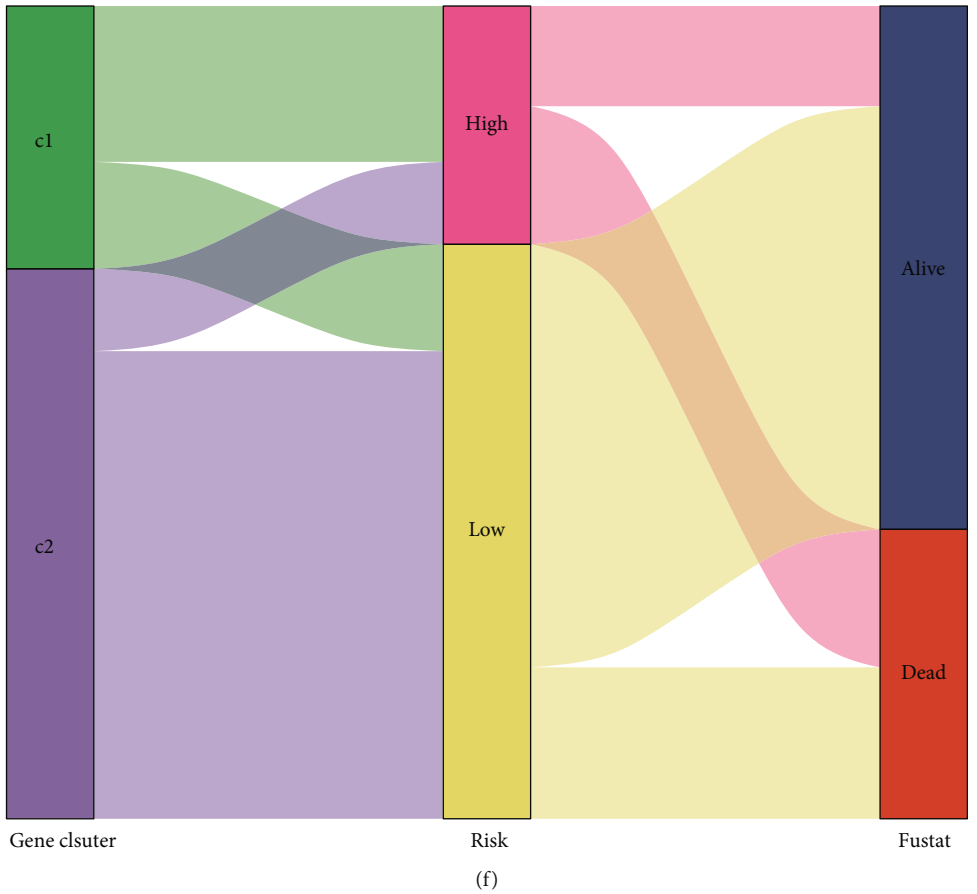

(f)

Figure 9: Drug-sensitive prediction and correlation between the cuproptosis-related molecular subtype and the cuproptosis-related signature. (a–d) Comparison of IC_{50} levels for sorafenib, cisplatin, paclitaxel, and gemcitabine between the low- and high-risk groups. (e) The distribution of risk scores between the molecular subtypes. (f) The Sankey diagram is used to present the distribution of molecular subtypes, risk status, and survival status.

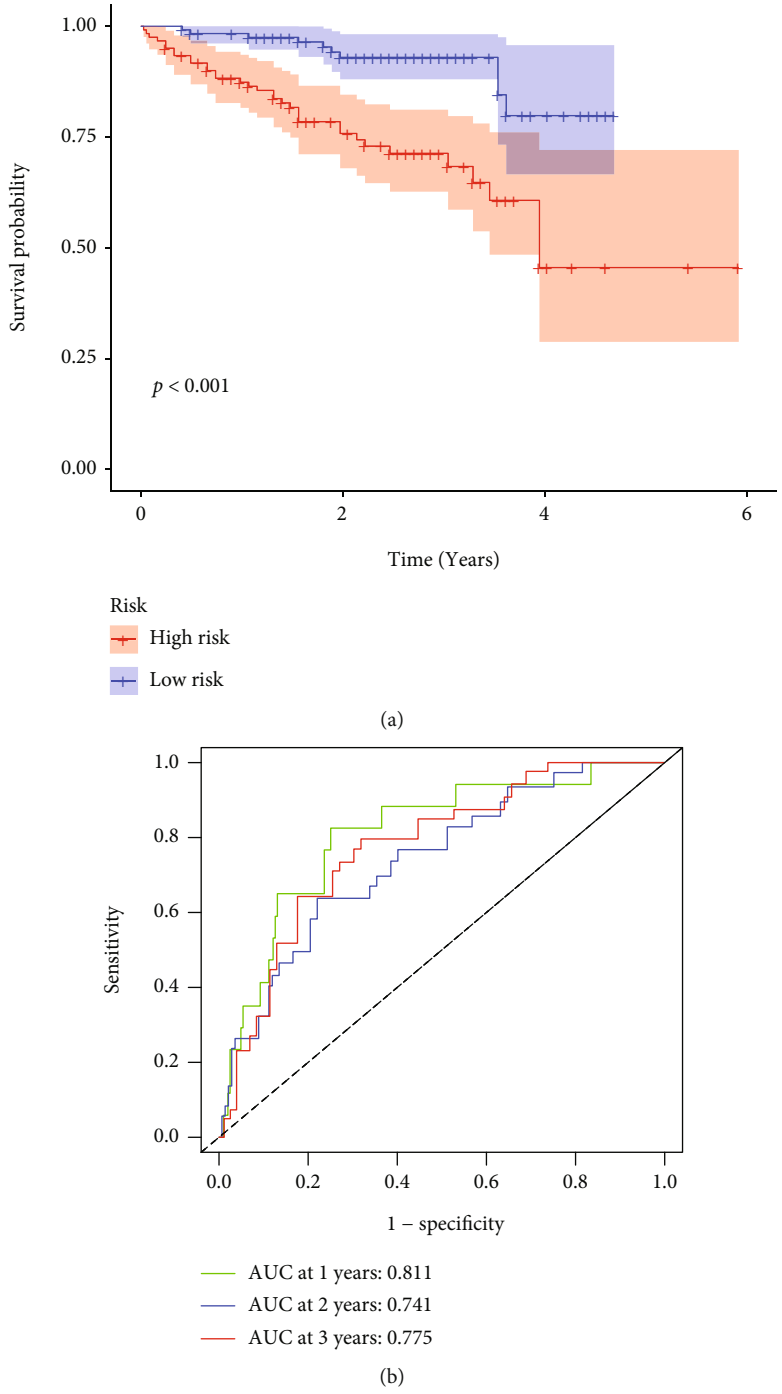

Figure 10: Continued.

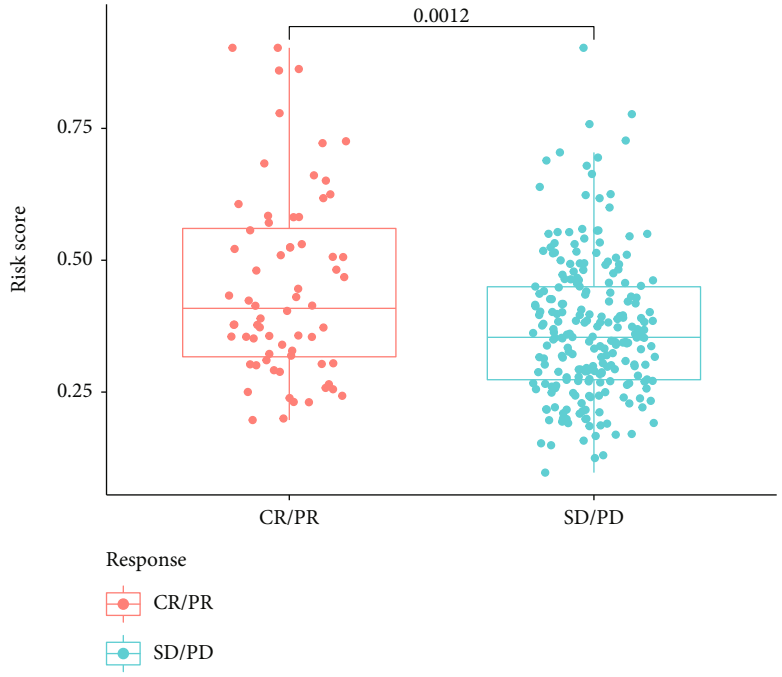

(c)

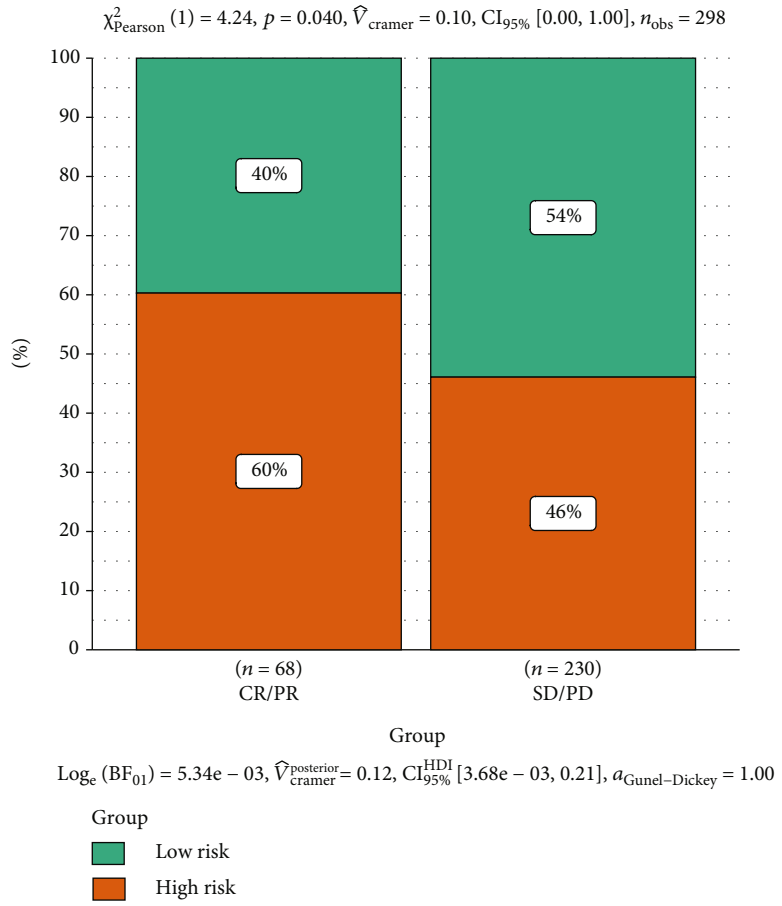

(d)

Figure 10: Validation of the signature in the LIRI-JP and IMvigor210 cohort. (a) K-M plot of the signature in the LIRI-JP cohort. (b) ROC curves for predicting 1-, 2-, and 3-year overall survival in the LIRI-JP cohort. (c and d) The ability of the signature to predict ICIs' response in the IMvigor210 cohort.

negative hits in the process of genome-wide CRISPR-Cas9 screen [15]. MTF1 was recently identified to be a propellant of tumor proliferation and metastasis in HCC cells and Hep3B-derived xenografts and was regulated by miR-148a-3p [37]. Knockdown or suppression of GLS impaired HCC cell proliferation and the expression level of GLS was modulated by nuclear factor-κB [38]. The expression of CDKN2A is inversely correlated with cyclin D-CDK4/6-retinoblastoma protein, which was a potential biomarker for ribociclib in HCC [39]. Genomic loss or deletion of CDKN2A was identified to be a risk factor for ICI therapy [40].

Advanced HCC patients have a paucity of curative systemic therapy options. Even though, clinical trials have shown that HCC patients could benefit from ICIs. Atezolizumab, a monoclonal antibody targeting PD-L1, combined with bevacizumab, prolonged the median progression-free survival to 6.8 months versus 4.3 months in the sorafenib group [5]. Pembrolizumab is an anti-PD-1 monoclonal antibody and was approved for advanced HCC which progressed after sorafenib by FDA. The median OS observed in pembrolizumab cohort, a cohort that included HCC patients who progressed after sorafenib treatment, was 12.9 months [41]. Nivolumab is used in combination with ipilimumab with an ORR of 32% and a median OS of 22.8 months [42]. Tremelimumab is a monoclonal antibody that binds to CTLA-4. The median OS in a phase I/II randomized clinical study of the combination of tremelimumab and durvalumab for advanced HCC was 18.73 months [43]. The expression level of immune checkpoint genes is considered to be associated with the response to ICIs [44]. HCC patients in the C1 cluster and high-risk group may be positive for ICIs since most of the immune checkpoint genes are highly expressed in this population. Cu was identified to be a PD-L1 regulator in HCC, when combined with disulfiram, a blocker of enzyme acetaldehyde dehydrogenase, it could upregulate the expression of PD-L1 [45]. TMB is defined as the total number of mutations detected per million bases [46]. A higher TMB level means more expressed neoantigens on the cell surface, hence these patients who harbor high-TMB levels are sensitive to immunotherapy [47]. The risk score is significantly positively correlated with the TMB level in our signature.

Immune cell infiltration influences the prognosis of HCC and ICI response. Regulatory T cells, which are significantly enriched in the high-risk group, are able to suppress the expression of PD-L1, promote HCC progression, and correlate with poor survival [48]. The infiltration of macrophages was strongly positively associated with the risk scores. Macrophages are known as immunosuppressive cells in the tumor immune microenvironment and are associated with a worse prognosis [49]. It was reported that Cu depletion is a negative factor for immune system, exemplifying that the activity of macrophages is decreased in Cu depletion rat model [50]. Integrated TIDE score is developed to evaluate the response of ICIs, and a higher TIDE score is associated with worse ICI response [51]. Patients in the high-risk group have a lower level of integrated TIDE score and may be sensitive to ICIs. ESTIMATE is a tool for predicting tumor purity, as well as the presence of stromal cell and immune cell [52]. There are no significant differences in tumor purity between the molecular subtypes and risk groups.

The signature is tested as an independent factor for HCC patients, and the AUC value of the signature in predicting OS shows satisfactory predictive ability in the TCGA-LIHC project and LIRI-JP cohort. Previous studies have constructed signatures associated with other cell death formats based on the TCGA-LIHC project. Yang and Jiang constructed a necroptosis-related signature with necroptosis-related genes, and the 1- and 3-year AUC values were 0.741 and 0.648, respectively [53]. Wu et al. constructed a pyroptosis-related signature with pyroptosis-related genes, and the 1- and 3-year AUC values were 0.785 and 0.71 [54], respectively, while 0.760 and 0.708 in a pyroptosis-related long noncoding RNAs (lncRNAs) signature [55]. The 1- and 3-year ACU values in ferroptosis-related gene signature are 0.8 and 0.668 [56]. Wang et al. established an autophagy-related gene signature, and the 1- and 3-year AUC value was 0.781 [57]. A ferroptosis and pyroptosis molecular subtype-related signature has the AUC values of 0.805, 0.806, and 0.751 for 1-, 3-, and 5-year [16].

The signature has the potential to predict drug response for HCC patients. HCC patients in the high-risk group are more likely to benefit from conventional anti-HCC agents and ICI therapies.

5. Conclusion

In summary, we presented the molecular characterization of CRGs in HCC and constructed a prognostic signature for HCC based on cuproptosis-related molecular subtype. Both the molecular subtype and the signature are strongly associated with cuproptosis and HCC prognosis, as well as exhibiting an abundant immune landscape.

Data Availability

The datasets used and/or analyzed in the current study are available in the article or supplementary material.

Disclosure

The authors report no conflicts of interest in this work.

Conflicts of Interest

The authors declare that they have no conflicts of interest.

Authors' Contributions

XJQ designed the study. XJQ, JYG, CSF, LHH, and CZ collected the data. XJQ, GMC, and JYG analyzed the data and drafted the manuscript. JL revised the final version of the manuscript. All the authors have read and approved the final version of the manuscript.

Acknowledgments

This study was supported by the Hunan Health and Health Commission General Project (20200949), the Changsha City Natural Science Foundation Project (kq2202453), the Excellent Youth Project of Hunan Provincial Education Department (21B0365), and the 2021 Hunan Clinical Medical Technology Innovation Guidance Project (2021SK51410).

Supplementary Materials

Supplementary 1. Supplementary Figure 1. Correlations between the CNV and gene expression of CRGs.

Supplementary 2. Supplementary Figure 2. Rank survey of the NMF analysis.

Supplementary 3. Supplementary Table 1. Detailed GSVA analysis of cuproptosis-related molecular subtype. Supplementary Table 2. Detailed GSVA analysis of cuproptosis-related signature. Supplementary Table 3. Detailed correlation analysis between risk scores and tumor-infiltrating immune cells.

References

[1] H. Sung, J. Ferlay, R. L. Siegel et al., "Global cancer statistics 2020: GLOBOCAN estimates of incidence and mortality worldwide for 36 cancers in 185 countries," *CA: a Cancer Journal for Clinicians*, vol. 71, no. 3, pp. 209–249, 2021.

[2] H. Zeng, W. Chen, R. Zheng et al., "Changing cancer survival in China during 2003-15: a pooled analysis of 17 population-based cancer registries," *The Lancet. Global Health*, vol. 6, no. 5, pp. e555–e567, 2018.

[3] A. Jemal, E. M. Ward, C. J. Johnson et al., "Annual report to the nation on the status of cancer, 1975-2014, featuring survival," *Journal of the National Cancer Institute*, vol. 109, no. 9, 2017.

[4] A. Villanueva, "Hepatocellular carcinoma," *The New England Journal of Medicine*, vol. 380, no. 15, pp. 1450–1462, 2019.

[5] R. S. Finn, S. Qin, M. Ikeda et al., "Atezolizumab plus bevacizumab in unresectable hepatocellular carcinoma," *The New England Journal of Medicine*, vol. 382, no. 20, pp. 1894–1905, 2020.

[6] U. Harkus, M. Wankell, P. Palamuthusingam, C. McFarlane, and L. Hebbard, "Immune checkpoint inhibitors in HCC: cellular, molecular and systemic data," *Seminars in Cancer Biology*, vol. 86, 2022.

[7] J. C. Nault and A. Villanueva, "Intratumor molecular and phenotypic diversity in hepatocellular carcinoma," *Clinical Cancer Research*, vol. 21, no. 8, pp. 1786–1788, 2015.

[8] S. M. Kalasekar, C. H. VanSant-Webb, and K. J. Evason, "Intratumor heterogeneity in hepatocellular carcinoma: challenges and opportunities," *Cancers*, vol. 13, no. 21, p. 5524, 2021.

[9] O. Miltiadous, D. Sia, Y. Hoshida et al., "Progenitor cell markers predict outcome of patients with hepatocellular carcinoma beyond Milan criteria undergoing liver transplantation," *Journal of Hepatology*, vol. 63, no. 6, pp. 1368–1377, 2015.

[10] A. Villanueva, Y. Hoshida, C. Battiston et al., "Combining clinical, pathology, and gene expression data to predict recurrence of hepatocellular carcinoma," *Gastroenterology*, vol. 140, no. 5, pp. 1501–1512.e2, 2011.

[11] D. Sia, Y. Jiao, I. Martinez-Quetglas et al., "Identification of an immune-specific class of hepatocellular carcinoma, based on molecular features," *Gastroenterology*, vol. 153, no. 3, pp. 812–826, 2017.

[12] A. Członkowska, T. Litwin, P. Dusek et al., "Wilson disease," *Nature reviews. Disease primers*, vol. 4, no. 1, p. 21, 2018.

[13] P. Ginès, A. Krag, J. G. Abraldes, E. Solà, N. Fabrellas, and P. S. Kamath, "Liver cirrhosis," *The Lancet*, vol. 398, no. 10308, pp. 1359–1376, 2021.

[14] Y. Tamai, M. Iwasa, A. Eguchi et al., "Serum copper, zinc and metallothionein serve as potential biomarkers for hepatocellular carcinoma," *PLoS One*, vol. 15, no. 8, article e0237370, 2020.

[15] P. Tsvetkov, S. Coy, B. Petrova et al., "Copper induces cell death by targeting lipoylated TCA cycle proteins," *Science*, vol. 375, no. 6586, pp. 1254–1261, 2022.

[16] J. Huo, J. Cai, G. Guan, H. Liu, and L. Wu, "A ferroptosis and pyroptosis molecular subtype-related signature applicable for prognosis and immune microenvironment estimation in hepatocellular carcinoma," *Frontiers in cell and developmental biology*, vol. 9, article 761839, 2021.

[17] J. Chen, Q. Tao, Z. Lang et al., "Signature construction and molecular subtype identification based on pyroptosis-related genes for better prediction of prognosis in hepatocellular carcinoma," *Oxidative Medicine and Cellular Longevity*, vol. 2022, Article ID 4494713, 20 pages, 2022.

[18] J. Zhang, R. Bajari, D. Andric et al., "The international cancer genome consortium data portal," *Nature Biotechnology*, vol. 37, no. 4, pp. 367–369, 2019.

[19] M. J. Goldman, B. Craft, M. Hastie et al., "Visualizing and interpreting cancer genomics data via the Xena platform," *Nature Biotechnology*, vol. 38, no. 6, pp. 675–678, 2020.

[20] S. Mariathasan, S. J. Turley, D. Nickles et al., "TGFβ attenuates tumour response to PD-L1 blockade by contributing to exclusion of T cells," *Nature*, vol. 554, no. 7693, pp. 544–548, 2018.

[21] J. Fu, K. Li, W. Zhang et al., "Large-scale public data reuse to model immunotherapy response and resistance," *Genome Medicine*, vol. 12, no. 1, p. 21, 2020.

[22] T. Li, J. Fu, Z. Zeng et al., "TIMER2.0 for analysis of tumor-infiltrating immune cells," *Nucleic Acids Research*, vol. 48, no. W1, pp. W509–w514, 2020.

[23] F. Finotello, C. Mayer, C. Plattner et al., "Molecular and pharmacological modulators of the tumor immune contexture revealed by deconvolution of RNA-seq data," *Genome Medicine*, vol. 11, no. 1, p. 34, 2019.

[24] J. Racle, K. de Jonge, P. Baumgaertner, D. E. Speiser, and D. Gfeller, "Simultaneous enumeration of cancer and immune cell types from bulk tumor gene expression data," *eLife*, vol. 6, 2017.

[25] B. Chen, M. S. Khodadoust, C. L. Liu, A. M. Newman, and A. A. Alizadeh, "Profiling tumor infiltrating immune cells with CIBERSORT," *Methods in Molecular Biology*, vol. 1711, pp. 243–259, 2018.

[26] D. Aran, Z. Hu, and A. J. Butte, "xCell: digitally portraying the tissue cellular heterogeneity landscape," *Genome Biology*, vol. 18, no. 1, p. 220, 2017.

[27] R. Dienstmann, G. Villacampa, A. Sveen et al., "Relative contribution of clinicopathological variables, genomic markers, transcriptomic subtyping and microenvironment features for

outcome prediction in stage II/III colorectal cancer," *Annals of oncology*, vol. 30, no. 10, pp. 1622–1629, 2019.

[28] M. Tamminga, T. J. N. Hiltermann, E. Schuuring, W. Timens, R. S. Fehrmann, and H. J. Groen, "Immune microenvironment composition in non-small cell lung cancer and its association with survival," *Clinical & translational immunology*, vol. 9, no. 6, article e1142, 2020.

[29] D. Miao, C. A. Margolis, N. I. Vokes et al., "Genomic correlates of response to immune checkpoint blockade in microsatellite-stable solid tumors," *Nature Genetics*, vol. 50, no. 9, pp. 1271–1281, 2018.

[30] H. Rizvi, F. Sanchez-Vega, K. La et al., "Molecular determinants of response to anti-programmed cell death (PD)-1 and anti-programmed death-ligand 1 (PD-L1) blockade in patients with non-small-cell lung cancer profiled with targeted next-generation sequencing," *Journal of Clinical Oncology*, vol. 36, no. 7, pp. 633–641, 2018.

[31] D. Tang, X. Chen, and G. Kroemer, "Cuproptosis: a copper-triggered modality of mitochondrial cell death," *Cell Research*, vol. 32, no. 5, pp. 417-418, 2022.

[32] M. Nurmamat, H. Yan, R. Wang et al., "Novel copper(II) complex with a 4-acylpyrazolone derivative and coligand induce apoptosis in liver cancer cells," *ACS Medicinal Chemistry Letters*, vol. 12, no. 3, pp. 467–476, 2021.

[33] C. I. Davis, X. Gu, R. M. Kiefer, M. Ralle, T. P. Gade, and D. C. Brady, "Altered copper homeostasis underlies sensitivity of hepatocellular carcinoma to copper chelation," *Metallomics : integrated biometal science*, vol. 12, no. 12, pp. 1995–2008, 2020.

[34] A. P. Fang, P. Y. Chen, X. Y. Wang et al., "Serum copper and zinc levels at diagnosis and hepatocellular carcinoma survival in the Guangdong liver cancer cohort," *International Journal of Cancer*, vol. 144, no. 11, pp. 2823–2832, 2019.

[35] A. Subastri, A. Suyavaran, E. Preedia Babu, S. Nithyananthan, R. Barathidasan, and C. Thirunavukkarasu, "Troxerutin with copper generates oxidative stress in cancer cells: its possible chemotherapeutic mechanism against hepatocellular carcinoma," *Journal of Cellular Physiology*, vol. 233, no. 3, pp. 1775–1790, 2018.

[36] Y. Wang, L. Zhang, and F. Zhou, "Cuproptosis: a new form of programmed cell death," *Cellular & Molecular Immunology*, vol. 19, no. 8, pp. 867-868, 2022.

[37] Z. Lyu, M. Yang, T. Yang, M. Ma, and Z. Yang, "Metal-regulatory transcription factor-1 targeted by miR-148a-3p is implicated in human hepatocellular carcinoma progression," *Frontiers in Oncology*, vol. 11, article 700649, 2021.

[38] M. Dong, L. Miao, F. Zhang et al., "Nuclear factor-κB p65 regulates glutaminase 1 expression in human hepatocellular carcinoma," *Oncotargets and Therapy*, vol. 11, pp. 3721–3729, 2018.

[39] F. P. Reiter, G. Denk, A. Ziesch et al., "Predictors of ribociclib-mediated antitumour effects in native and sorafenib-resistant human hepatocellular carcinoma cells," *Cellular Oncology*, vol. 42, no. 5, pp. 705–715, 2019.

[40] S. I. Gutiontov, W. T. Turchan, L. F. Spurr et al., "CDKN2A loss-of-function predicts immunotherapy resistance in non-small cell lung cancer," *Scientific Reports*, vol. 11, no. 1, p. 20059, 2021.

[41] A. X. Zhu, R. S. Finn, J. Edeline et al., "Pembrolizumab in patients with advanced hepatocellular carcinoma previously treated with sorafenib (KEYNOTE-224): a non-randomised, open-label phase 2 trial," *The Lancet Oncology*, vol. 19, no. 7, pp. 940–952, 2018.

[42] T. Yau, Y. K. Kang, T. Y. Kim et al., "Efficacy and safety of nivolumab plus ipilimumab in patients with advanced hepatocellular carcinoma previously treated with sorafenib: the CheckMate 040 randomized clinical trial," *JAMA Oncology*, vol. 6, no. 11, article e204564, 2020.

[43] R. K. Kelley, B. Sangro, W. Harris et al., "Safety, efficacy, and pharmacodynamics of tremelimumab plus durvalumab for patients with unresectable hepatocellular carcinoma: randomized expansion of a phase I/II study," *Journal of Clinical Oncology*, vol. 39, no. 27, pp. 2991–3001, 2021.

[44] B. Sangro, I. Melero, S. Wadhawan et al., "Association of inflammatory biomarkers with clinical outcomes in nivolumab- treated patients with advanced hepatocellular carcinoma," *Journal of Hepatology*, vol. 73, no. 6, pp. 1460–1469, 2020.

[45] B. Zhou, L. Guo, B. Zhang et al., "Disulfiram combined with copper induces immunosuppression via PD-L1 stabilization in hepatocellular carcinoma," *American Journal of Cancer Research*, vol. 9, no. 11, pp. 2442–2455, 2019.

[46] A. Rizzo and G. Brandi, "Biochemical predictors of response to immune checkpoint inhibitors in unresectable hepatocellular carcinoma," *Cancer treatment and research communications*, vol. 27, article 100328, 2021.

[47] A. M. Goodman, S. Kato, L. Bazhenova et al., "Tumor mutational burden as an independent predictor of response to immunotherapy in diverse cancers," *Molecular Cancer Therapeutics*, vol. 16, no. 11, pp. 2598–2608, 2017.

[48] B. Niu, S. Wei, J. Sun, H. Zhao, B. Wang, and G. Chen, "Deciphering the molecular mechanism of tetrandrine in inhibiting hepatocellular carcinoma and increasing sorafenib sensitivity by combining network pharmacology and experimental evaluation," *Pharmaceutical Biology*, vol. 60, no. 1, pp. 75–86, 2022.

[49] W. Zhang, X. D. Zhu, H. C. Sun et al., "Depletion of tumor-associated macrophages enhances the effect of sorafenib in metastatic liver cancer models by antimetastatic and antiangiogenic effects," *Clinical Cancer Research*, vol. 16, no. 13, pp. 3420–3430, 2010.

[50] U. Babu and M. L. Failla, "Respiratory burst and candidacidal activity of peritoneal macrophages are impaired in copper-deficient rats," *The Journal of Nutrition*, vol. 120, no. 12, pp. 1692–1699, 1990.

[51] P. Jiang, S. Gu, D. Pan et al., "Signatures of T cell dysfunction and exclusion predict cancer immunotherapy response," *Nature Medicine*, vol. 24, no. 10, pp. 1550–1558, 2018.

[52] K. Yoshihara, M. Shahmoradgoli, E. Martínez et al., "Inferring tumour purity and stromal and immune cell admixture from expression data," *Nature Communications*, vol. 4, no. 1, p. 2612, 2013.

[53] H. Yang and Q. Jiang, "A multi-omics-based investigation of the immunological and prognostic impact of necroptosis-related genes in patients with hepatocellular carcinoma," *Journal of Clinical Laboratory Analysis*, vol. 36, no. 4, article e24346, 2022.

[54] Z. H. Wu, Z. W. Li, D. L. Yang, and J. Liu, "Development and validation of a pyroptosis-related long non-coding RNA signature for hepatocellular carcinoma," *Frontiers in cell and developmental biology*, vol. 9, article 713925, 2021.

[55] Z. K. Liu, K. F. Wu, R. Y. Zhang et al., "Pyroptosis-related LncRNA signature predicts prognosis and is associated with

immune infiltration in hepatocellular carcinoma," *Frontiers in Oncology*, vol. 12, article 794034, 2022.

[56] J. Y. Liang, D. S. Wang, H. C. Lin et al., "A novel ferroptosis-related gene signature for overall survival prediction in patients with hepatocellular carcinoma," *International Journal of Biological Sciences*, vol. 16, no. 13, pp. 2430–2441, 2020.

[57] J. Wang, Y. Miao, J. Ran, Y. Yang, Q. Guan, and D. Mi, "Construction prognosis model based on autophagy-related gene signatures in hepatocellular carcinoma," *Biomarkers in Medicine*, vol. 14, no. 13, pp. 1229–1242, 2020.